Bioconjugate Chemistry

pubs.acs.org/bc

Review

State of the Art in Radiolabeling of Antibodies with Common and Uncommon Radiometals for Preclinical and Clinical Immuno-PET

Marion Chomet, Guus A. M. S. van Dongen, and Danielle J. Vugts*

Cite This: *Bioconjugate Chem.* 2021, 32, 1315−1330

Read Online

ACCESS | Metrics & More | Article Recommendations

ABSTRACT: Inert and stable radiolabeling of monoclonal antibodies (mAb), antibody fragments, or antibody mimetics with radiometals is a prerequisite for immuno-PET. While radiolabeling is preferably fast, mild, efficient, and reproducible, especially when applied for human use in a current Good Manufacturing Practice compliant way, it is crucial that the obtained radioimmunoconjugate is stable and shows preserved immunoreactivity and *in vivo* behavior. Radiometals and chelators have extensively been evaluated to come to the most ideal radiometal−chelator pair for each type of antibody derivative. Although PET imaging of antibodies is a relatively recent tool, applications with ^{89}Zr, ^{64}Cu, and ^{68}Ga have greatly increased in recent years, especially in the clinical setting, while other less common radionuclides such as ^{52}Mn, ^{86}Y, ^{66}Ga, and ^{44}Sc, but also ^{18}F as in [^{18}F]AlF are emerging promising candidates for the radiolabeling of antibodies. This review presents a state of the art overview of the practical aspects of radiolabeling of antibodies, ranging from fast kinetic affibodies and nanobodies to slow kinetic intact mAbs. Herein, we focus on the most common approach which consists of first modification of the antibody with a chelator, and after eventual storage of the premodified molecule, radiolabeling as a second step. Other approaches are possible but have been excluded from this review. The review includes recent and representative examples from the literature highlighting which radiometal−chelator−antibody combinations are the most successful for *in vivo* application.

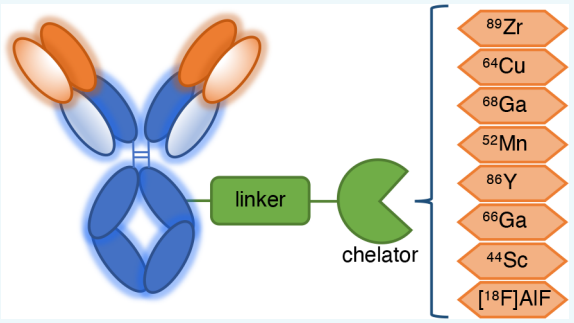

■ ANTIBODIES AND IMMUNO-PET

The Emerging Role of Antibodies. Monoclonal antibodies (mAbs) have emerged as next-generation therapeutic drugs, especially for the treatment of cancer, due to their high specificity toward certain antigens. Ideally, the target should be tumor selective to avoid binding of mAbs to healthy organs expressing the same target.[1] While initially, only unconjugated IgGs (mostly of IgG1 subclass) were developed for therapy, mainly used for blocking signal transduction of tyrosine kinases or other membrane receptor targets involved in oncology and other diseases,[2] the trend in the past decade is set on development of antibody−drug conjugates (ADC), multispecific mAbs, immune checkpoints inhibitors, and also mAb fragments such as single domain antibodies, nanobodies, and antibody mimetics such as affibodies (Figure 1; in this review collectively called "antibodies").[3−5] The development of this wide range of antibodies is accompanied by questions concerning their *in vivo* behavior, pharmacokinetics, and targeting efficiency. The growing field of mAb development is comprehensively described in the journal mAbs that publishes yearly an update on "antibodies to watch", showing that between 2010 and the end of 2019, the cumulative number of antibodies approved in the US and EU has almost tripled resulting in a total of about 80 approvals. About 50% of the antibody therapeutics currently in phase II or III clinical studies are evaluated in noncancer applications.[6,7]

Positron Emission Tomography (PET) as a Tool to Evaluate Antibodies. Positron emission tomography (PET) is not only used for diagnosis and response monitoring using [^{18}F]FDG, but has also become a highly valuable imaging technique helping to understand the behavior of antibodies at an early stage during development by evaluating the radiolabeled antibodies in so-called immuno-PET imaging studies. Immuno-PET is now increasingly used in early-phase clinical trials for making go/no go decisions based on results obtained with a limited number of patients. In this way, immuno-PET enables steering drug design and contributes to drug and patient selection, and as a consequence, the development of new medicines is sped up in a cost-effective way. Thanks to its high resolution, sensitivity, and better quantification ability, PET is preferred over single-photon emission computed

Special Issue: State-of-the-Art of Radiometal-based Bioconjugates for Molecular Imaging and Radiotherapy

Received: March 18, 2021
Revised: April 28, 2021
Published: May 11, 2021

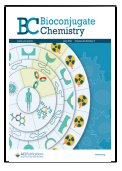

https://doi.org/10.1021/acs.bioconjchem.1c00136
Bioconjugate Chem. 2021, 32, 1315−1330

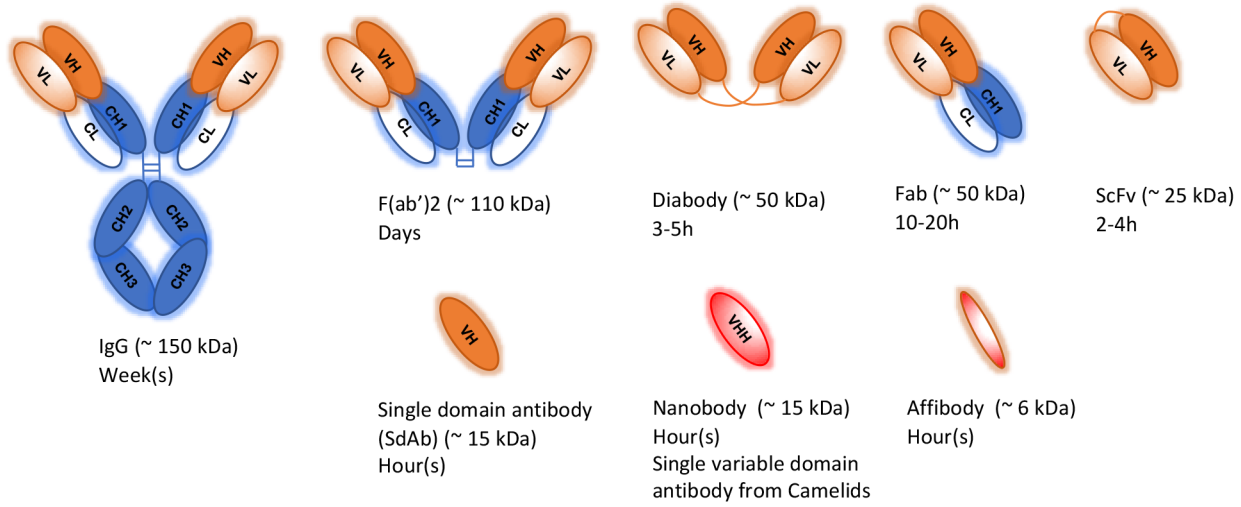

Figure 1. Representation of a monoclonal antibody, isotype IgG, containing two light (L) and heavy (H) chains maintained together via disulfide bonds. The variable region (Fv) is composed of the variable heavy (VH) and variable light (VL) chains. VH and VL are together with the constant light and heavy chain 1 (CL and CH1) constituting the Fab region. CH2 and CH3 are the constant region (Fc). Many of the smaller molecular weight antibody fragments have been engineered from this general structure and the ones discussed in this review are summarized here, including the antibody mimetic affibody. Approximative molecular weight and *in vivo* biological half-life are indicated.

Table 1. Physical Characteristics and Production Route of PET Radionuclides Discussed in This Review

radionuclide	production route	half-life	Eβ max (kev)	mean range in water (mm)	β^+ (%)	characteristic main transition γ (keV)
^{52}Mn	Cyclotron ^{52}Cr(p,n) ^{52}Mn	5.6 d	β^+ (573.3)	0.6	$\varepsilon^+\beta^+$ (100%)	434.1 (100.0%)[b]
					β^+ (29.4%)	935.5 (94.9%)
						744.2 (90.3%)
						333.6 (5.1%)
^{89}Zr	Cyclotron ^{89}Y(p,n) ^{89}Zr	78.4 h	β^+ (902)	1.2	$\varepsilon^+\beta^+$ (100%)	909 (99.9%)
					β^+ (22.7%)	
^{86}Y	Cyclotron ^{86}Sr(p,n) ^{86}Y	14.74 h	β^+ (3153)	1.9	$\varepsilon^+\beta^+$ (100%)	1076.6 (83.0%)[b]
					β^+ (31.9%)	627.7 (32.6%)
						1153.0 (30.6%)
						777.4 (22.4%)
						1920.7 (20.8%)
						1854.4 (17.2%)
						443.1 (16.9%)
						703.3 (15.4%)
						645.9 (9.2%)
^{64}Cu	Cyclotron ^{64}Ni(p,n) ^{64}Cu	12.7 h	β^+ (653.0)	0.7	$\varepsilon^+\beta^+$ (61.5%)	n.a.[a]
			β^- (579.4)		β^+ (17.6%)	
					β^- (38.5%)	
^{66}Ga	Cyclotron ^{66}Zn(p,n)^{66}Ga	9.49 h	β^+ (4153)	9.3	$\varepsilon^+\beta^+$ (100%)	1039.2 (37.0%)[b]
					β^+ (56.5%)	2751.9 (23.3%)
						833.5 (5.9%)
						2189.6 (5.6%)
^{44}Sc	Cyclotron ^{44}Ca(p,n) ^{44}Sc-generator ^{44}Sc(p,2n) ^{44}Ti → ^{44}Sc	4.0 h	β^+(1473.5)	2.3	$\varepsilon^+\beta^+$ (100%)	1157.0 (99.9%)
					β^+ (94.3%)	
^{18}F−Al	Cyclotron ^{18}O(p,n) ^{18}F	109.8 min (^{18}F)	β^+ (633.5)	0.6	β^+ (96.9%)	n.a.[a]
^{68}Ga	Generator ^{68}Ge → ^{68}Ga	67.7 min	β^+ (1899.1)	2.9	$\varepsilon^+\beta^+$ (100%)	n.a.[a]
					β^+ 90%	

[a]Nonapplicable: ≤1% [b]Energies with an abundance <5% left out.

https://doi.org/10.1021/acs.bioconjchem.1c00136
Bioconjugate Chem. 2021, 32, 1315−1330

tomography (SPECT), while the availability of preclinical and clinical PET cameras strongly increased during the past decade.[8]

Radionuclides for PET Imaging of Antibodies. Antibodies are proteinaceous molecules typically ranging from a few to about 150 kDa in size. As a result, their pharmacokinetics also range from short (less than an hour serum half-life) to long (days) blood circulating half-life. To enable *in vivo* characterization of an antibody with a PET camera, a positron emitter has to be attached in a stable and inert way. For this purpose, radiometals are particularly interesting, since they can be used in combination with antibodies that have been premodified by means of a bifunctional chelating agent, allowing facile single-step radiolabeling. In addition, radiometals of such constructs possess residualizing properties. Zirconium-89, copper-64, and gallium-68 have emerged over the years as the preferred radiometals for radiolabeling of antibodies, because of their physical properties, availability, costs, and ease of radiolabeling (see Tables 1 and 2).[9,10] The half-life of zirconium-89 ($t_{1/2}$ = 78.4 h) matches the biological half-life of long-circulating large (slow kinetic) molecules like intact mAbs (Figure 1), while copper-64 possesses an intermediate half-life ($t_{1/2}$ = 12.7 h) that can be used for antibody fragments with medium to relatively fast kinetics. On the contrary, radionuclides such as gallium-68 ($t_{1/2}$ = 67.7 min) are preferred for antibody fragments and mimetics with a very short serum half-life such as nanobodies or affibodies (see Table 1). Although ^{89}Zr, ^{64}Cu, and ^{68}Ga are the most commonly used radiometals for radiolabeling of antibodies, none of them are perfect, triggering research on other emerging radiometals such as manganese-52, yttrium-86, gallium-66, and scandium-44. Moreover, recent advances in [^{18}F]AlF radiochemistry expand the options for radiolabeling of antibodies with ^{18}F. ^{18}F is by far the most commonly used PET radionuclide thanks to its short half-life (110 min), its ideal physical properties as extensively shown in small molecule imaging, and its increasing availability. Finally, the application of matching theranostic pairs (SPECT or PET for imaging combined with radionuclide therapy) is an interesting re-emerging field in nuclear medicine. Around 20 years ago, a first wave has been observed in the use of theranostics, which was followed by near-abandonment.[11] In recent years, there has been renewed interest in theranostics as exemplified by, e.g., PSMA imaging and therapy.[12] The concept of matching pairs relies on two different approaches, either using the same targeting ligand in combination with two different isotopes (a diagnostic and a therapeutic one) of the same element or using two different radionuclides.[13] The first approach is in theory ideal to assess biodistribution, target accumulation, and redistribution of the radioactive and nonradioactive catabolites to fully predict therapeutic response by dosimetric analysis. In the second approach, the diagnostic radiotracer is used as a scouting agent for the therapeutic one, but this requires that both tracers present the same *in vivo* behavior.

Bifunctional Chelators (BFCs) and Conjugation Strategies. *(i) Antibodies are mostly radiolabeled with radiometals via a bifunctional chelator (BFC) consisting of a chelator to coordinate the radiometal and a linker to allow coupling to the antibody.* Antibodies are generally modified by either random or site-specific conjugation to lysines using activated carboxylic acids and isothiocyanates or to thiols using maleimides.[14] For details on recent advances in site-specific conjugation methods, click chemistry, and pretargeting strategies, we refer to the reviews of Morais and Ma,[15] Adumeau et al.,[16,17] Meyer et al.,[18] and to the section on "new conjugation strategies" from the review of Wei et al. from 2020.[19] BFCs should be coupled in an inert and stable way, not affecting the protein integrity, immunoreactivity, and *in vivo* biodistribution of the antibody and avoiding the release of the radionuclide. Several aspects are of importance to guarantee inertness. BFC conjugation conditions should be relatively mild to avoid alteration of the protein integrity.

Among others, the pH of the conjugation reaction mixture is usually kept between 7 and 9, while high reaction temperature (>50 °C) can seriously alter the secondary and tertiary structures of the antibody and should be avoided to preserve antibody integrity. After BFC conjugation, usually a purification step is needed (i.e., via size exclusion) to remove uncoupled chelator molecules and to improve subsequent radiolabeling yields.

(ii) Conjugation to or near the antigen binding domain of the antibody should be avoided to prevent impairment of immunoreactivity. The larger the antibody is, the more lysines are available outside the antigen binding region, thus reducing the chance of impaired immunoreactivity. This becomes more challenging for small antibody derivatives like nanobodies where a site-specific conjugation might be preferred to avoid conjugation of the BFC to an amino acid to or near the complementary-determining regions (CDR) of the antibody. Site-specific coupling harbors the advantage of controlling where the antibody will be modified, thus resulting in a homogeneous product. This approach, however, requires either engineering of antibodies to introduce functional chemical group for BFC coupling or pretreating the antibody before BFC conjugation to obtain reaction sites.

(iii) The number of chelator molecules coupled per antibody molecule should be kept within limits, avoiding alteration of the normal biodistribution of the mAb. It is generally assumed that one to two chelators per antibody on average do not interfere with the normal biodistribution of the antibody. Apart from the number of chelators coupled, various factors can also be responsible for disturbing the pharmacokinetics of the antibody such as the overall charge, isoelectric point, and hydrophilicity of the radiolabeled molecule. Furthermore, the intramolecular positions of the lysine and thiol functions available for conjugation with the BFC are important. While modification on the Fc part of the mAb should be preferred, conjugation to the variable domain should be avoided to exclude impairment of the immunoreactivity of the mAb toward the antigen binding site.

Quality Controls. Radiotracers based on antibodies usually undergo quality control tests directly after radiolabeling and subsequent purification and formulation. Among the release specifications for preclinical and clinical application are radiochemical purity, protein integrity, and maintenance of biological properties such as antigen binding. Furthermore, storage conditions must be established and a shelf life should be set for which those release specifications are proven to be preserved.

Formulation of radiolabeled antibodies is typically done in aqueous buffers, and quality controls are performed by HPLC (i.e., size exclusion chromatography) or SDS-PAGE using radiodetection to determine the radiochemical purity and protein integrity. TLC or spin filter analysis, based on molecular weight size-exclusion separation, is used to assess

https://doi.org/10.1021/acs.bioconjchem.1c00136
Bioconjugate Chem. 2021, 32, 1315−1330

Table 2. Representative Radiolabeling Conditions for Antibodies or Antibody Derivatives Evaluated in Recent Preclinical Studies with ^{89}Zr, ^{64}Cu, ^{68}Ga, and [^{18}F]AlF[a]

radionuclide	chelator (-linker)	antibody derivatives	conjugation conditions	radiolabeling conditions	ref
^{89}Zr	DFO(-NCS)	mAb	3 equiv; 30 min; 37 °C; pH ∼ 9	1 h; RT; pH ∼ 7	14,23−27,63
	DFO(-maleimide)	mAb	60 equiv; 60 min; RT; pH not indicated	1 h; RT; pH ∼ 7	64
		Affibodies	34−40 equiv; 2 h; 40 °C; pH ∼ 7.4 (in PBS)	1 h; RT; pH ∼ 7	65
	DFO(-N-suc-TFP ester)	mAb	2 equiv; 30 min; RT; pH ∼ 9; Fe removal with EDTA; 30 min; 35 °C pH 4.3−4.5	1 h; RT; pH ∼ 7	63,66,67
	DFO*(-NCS)	mAb	3−5 equiv; 30−45 min; 37 °C; pH ∼ 9	1 h; RT; pH ∼ 7	47,50
	DFOSq	mAb	3−20 equiv; overnight; RT; pH ∼ 9	25 min−1 h; RT; pH ∼ 7	50,52,68
	DFO*Sq	mAb	5 equiv; overnight; RT; pH ∼ 9	1 h; RT; pH ∼ 7	50
	3,4,3-(LI-1,2-HOPO)-(NCS)	mAb	5 equiv; 1 h; 37 °C; pH ∼ 9	RT; 1−3 h; pH ∼ 7	37
	DFO-cyclo*-(NCS)	mAb	30 equiv; overnight; 37 °C; pH 8.4	30 min; RT; pH ∼ 7	48
^{64}Cu	DOTA(-maleimido-monoamide)	Affibodies	15 equiv; 2 h; RT; pH 7.4	1 h; 40 °C; pH 6	69
	DOTA(-NCS)	mAb	10 equiv; overnight; 37 °C; pH 8.5	1 h; 40 °C; pH 5.5	70
	DOTA(−NHS)	mAb	10−30 equiv; 1 h (or overnight at 4 °C); RT to 37 °C; pH 7.0−8.5	30 min−1 h; 37−43 °C; pH 5.0−7.0	71−73
	NOTA-(NCS)	Fab and F(ab′)2	5−10 equiv; 1−2 h, RT to 37 °C; rarely 24 h or overnight at 4 °C; pH 8.0−9.2	30 min (15 min to 1 h); 37−40 °C; mostly pH 5.0 (4.5−5.5)	74−99
		scFv	25 equiv; overnight; 4 °C; pH 9	1 h; 40 °C; pH 6.5	
		Nanobody	20 equiv; 2 h; RT; pH 8.7	10 min; RT; pH 5	
		mAb	Mostly 5−25 equiv; 1−3 h ± overnight at 4 °C; RT to 37 °C; pH 8.0−9.0,	30 min−1 h; RT to 37 °C; pH 4.5−6.5	
	NOTA(-NHS)	mAb	50−55 eq ; 1 h RT or overnight at 4 °C; pH 7.5−8.6	1 h; 37−42 °C; pH 5.0.-6.0	
	NOTA-maleimide	Diabody	Site specific with maleimide, pH 7.4	1 h; 40 °C; 1 h; pH 6	
	NODAGA(-NCS)	Fab	equiv not indicated; 1 h; 37 °C; pH 8.5	20 min; 37 °C; pH 5.5	100−105
		F(ab′)2	20 equiv; 3 h; RT; pH 9.5	30 min; RT; pH 5.5	
		mAb	20 equiv; 1 h; RT; pH 9	1 h; 52 °C; pH 5−6	
		mAb	25 equiv; 16 h; 4 °C; in PBS ∼ pH 7.4	30 min; 42 °C; pH 6−7	
	NODAGA(-NHS)	mAb	55 equiv; overnight; 4 °C pH ∼ 7	1 h; 42 °C, pH 7	
	PCTA(-NCS)	mAb	10 equiv; RT 2 h then 4 °C overnight; pH 8.5	1 h; RT; pH 6.5	106−108
		mAb	5 equiv; overnight; 37 °C; pH 8.5	1 h; 40 °C; pH 5.5	
	CB-TE2A with a Gly-Glu-Glu-Glu spacer	Affibodies	10 equiv; 2 h; RT; no pH indicated	45 min; 95 °C; pH 5.6	109
	phosphinate PS(-NCS)	mAb	40 equiv; 2 h RT, then 4 °C for 12 h; pH 8.5	40 min; 37 °C; pH 5.5	110
	Sarcophagine derivatives	mAb fragments	250 equiv chelator; 500 equiv EDC; RT? (not indicated); 30 min; pH 5	30 min; 25 °C; pH 5	111
^{68}Ga	DOTA(-MMADOTA) (maleimide-monoamide)	Affibody	Site-specific, overnight; 37 °C; pH 5.5	15 min, 80 °C; pH 3.9	112
	NOTA-(NCS)	mAb	25 equiv; 16 h; RT; pH 9	pH 5.0, 5 min, RT	113
		Nanobody	10−20 equiv; 2−2.5 h; RT; pH 8.5−8.7	5−10 min; RT; pH 4.7−5.0,	114−116
		F(ab′)2	200 equiv; overnight; 4 °C pH 9	10−15 min; RT to 39 °C; pH ∼ 5.0−5.5	117,118
		Single domain antibody	∼10−20 equiv; 2−18 h; RT; pH 8.5−8.7	10 min; RT; pH 4.0−5.0	119−121
	NOTA(−NHS)	mAb	3 equiv; overnight; 4 °C; in water (pH ∼ 7)	30 min; RT; pH 3.7	122
		scFv	∼3.5 equiv, overnight, 4 °C; pH not indicated	30 min; RT; pH 3.7	123
	photoactivable chelate, HBED-CC-PEG3-ArN3	mAb	5 equiv; LED irradiated 10 min, RT; pH 8−9	RT; reaction followed by TLC; pH 4.4	124
	DFO comparison with ^{89}Zr DFO-derivative	scFv	3 equiv; 30 min, 37 °C in 50 mM $NaHCO_3$	5 min; RT but low chelator:protein ratio obtained (0.14 DFO-NCS per scFv); pH 5.5	125

https://doi.org/10.1021/acs.bioconjchem.1c00136
Bioconjugate Chem. 2021, 32, 1315−1330

Table 2. continued

radionuclide	chelator (-linker)	antibody derivatives	conjugation conditions	radiolabeling conditions	ref
[^{18}F]AlF	NOTA(-MMA)	Affibody	20 equiv; site specific, 1−2 h, 37 °C; pH 7.4	15 min; 100 °C; pH 4	126, 127
	phenyloxadiazolyl methylsulfone derivatives (PODS) chelators: NOTA- and NODAGA-PODS-	Affibody	15 equiv; site specific with maleimide, 1 h; 37 °C; pH 7	15 min; 100 °C; pH 4	128
	RESCA as (±)-H3RESCA-TFP	mAb and Nanobody	12−15 equiv; 2−3 h; RT; pH 8.6	12 min; RT; pH 4.5	129
	(±)-H3RESCA-maleimide compared with MMA-NOTA	Affibody	1 equiv; site specific; 90 min; RT; pH 7.5	15 min, 37 °C (RESCA) or 100 °C (NOTA); pH 4	129

[a]The number of molar equivalents used (chelator-to-antibody ratio) in conjugation reactions is abbreviated as "equiv" and room temperature is abbreviated as RT. Chemical structures of the chelators are presented in Figure 2.

the radiochemical purity as well. Finally, binding assays need to be developed to check that the immunoreactivity (binding to the antigen) of the radioimmunoconjugate is preserved via either cell-based or ELISA-like assays.[20] Additionally, production of a radiotracer for clinical use needs to follow Good Manufacturing Practice (GMP) guidelines in a clean and controlled environment with a reproducible and validated manufacturing process and well-defined releasing criteria.[21]

In this review, an overview of radiometal-labeled antibodies that have been evaluated *in vivo* in the past five years will be given. The constructs selected range from nanobodies to monoclonal antibodies (mAbs) (Figure 1) labeled with the often used radiometals ^{89}Zr, ^{64}Cu, and ^{68}Ga; with less common radionuclides ^{52} Mn, ^{86}Y, ^{66}Ga, and ^{44}Sc; or with ^{18}F using chelated aluminum as the metal. We will discuss practical considerations with respect to the chelators used and strategies for complexation of radiometals as well as the radiolabeling conditions of antibodies with radiometals. Approaches that consist of labeling of chelators first (prelabeling approach), followed by coupling to the biological molecule, are excluded from this review.

RADIOMETALS EVALUATED IN IMMUNO-PET

^{89}Zr. Thanks to its half-life of 78.41 h, ^{89}Zr has been extensively used for the radiolabeling of mAbs. ^{89}Zr is readily available via commercial suppliers, produced in a cyclotron via the ^{89}Y(p,n)^{89}Zr nuclear reaction and obtained as ^{89}Zr-oxalate ($[^{89}Zr(C_2O_4)_4]^{4-}$). ^{89}Zr decays via β^+ emission (23%) and electron capture (77%) to ^{89m}Y ($t_{1/2}$ = 15.7 s) and finally to ^{89}Y via γ emission of 909 keV which does not interfere with PET imaging (see Table 1).[22]

Remarkably, desferrioxamine (DFO) is still the only chelator used in clinical studies, which can be explained by the fact that it is a well-known chelator that has been used safely for decades as an antidote for iron overload. Furthermore, coupling reactions with commercially available bifunctional derivatives of DFO (TFP-*N*-suc-DFO and DFO-NCS) have been extensively reported with well-described[23−26] and GMP compliant procedures.[27,28] Recently, some comprehensive reviews have been published by Wei et al.,[29] Yoon et al.,[30] and van Dongen et al.[2] on the preclinical and clinical use of ^{89}Zr-immuno-PET.

Zirconium-89 is typically present in solution as Zr^{4+}, and is a hard Lewis acid with strong affinity for hard Lewis bases such as oxygen. An octadentate coordination sphere is preferred, while DFO is only able to provide hexadendate coordination. Two additional coordinating ligands are supposed to be needed for optimal stabilization of the ^{89}Zr-complex.[31,32] This has led to suboptimal stability with DFO in preclinical *in vivo* models and uptake of free ^{89}Zr in bones. Whether this is a topic of concern in the clinical setting, especially regarding bone dosimetry at late time points and possible misdiagnosis in case of bone metastasis, is not clear yet and remains to be investigated.[31−37] Multiple research groups have developed octadentate chelators for ^{89}Zr to solve this issue while keeping synthesis, coupling, and radiolabeling conditions facile and mild. Research in the field on new chelators for ^{89}Zr has been extensively reported in reviews;[9,38−45] see Table 2 and Figure 2 for an overview of bifunctional chelators recently evaluated in a preclinical setting.

One of the newly developed octadentate chelators is DFO*,[46] a derivative of DFO with an additional fourth hydroxamate group in comparison with DFO. DFO*-mAb

https://doi.org/10.1021/acs.bioconjchem.1c00136
Bioconjugate Chem. 2021, 32, 1315−1330

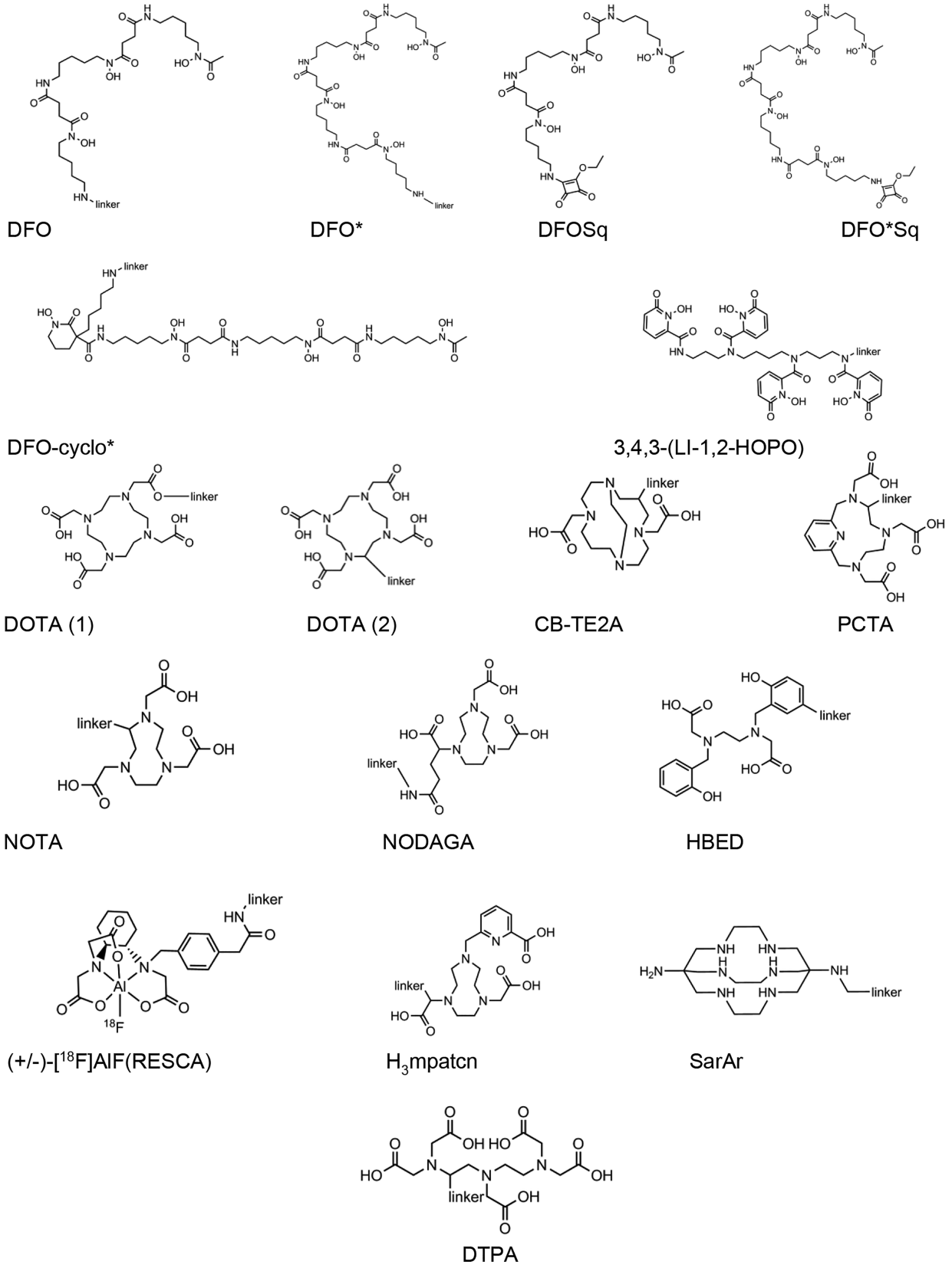

Figure 2. Chemical structures of main chelators discussed in this review. If applicable, the most common position for conjugation via a linker has been indicated. [^{18}F]AlF has been indicated to illustrate the special coordination geometry of RESCA.

complexes demonstrated improved stability, *in vitro* as well as *in vivo*, with clearly less bone uptake.[47−51] Moreover, DFO*, DFO*-NCS, and DFO*-maleimide have recently become commercially available, which should greatly facilitate clinical translation. In a recent study,[50] DFO* was compared with DFOSq, a chelator introduced by Rudd et al. that also showed

https://doi.org/10.1021/acs.bioconjchem.1c00136
Bioconjugate Chem. 2021, 32, 1315−1330

promising preliminary results,[52] and DFO*Sq, a hybrid chelator used to better understand the influence of the extra hydroxamate group of DFO* and the Squaramide. *In vivo* uptake in bones was, however, unfavorable for DFOSq in comparison with the DFO* chelators and density function theory (DFT) measurements demonstrated that DFOSq is actually a seven-coordinate complex and thus not able to fully coordinate ^{89}Zr.[53]

Two other bifunctional chelators, *p*-SCN-Bn-HOPO (based on 3,4,3-(LI-1,2-HOPO))[37] and DFO-cyclo*-*p*Phe-NCS[48] have shown promising preclinical results. However, the use of *p*-SCN-Bn-HOPO is hampered by the rather complicated synthesis of the BFC, and no clinical application has been reported yet.[54] DFO-cyclo*-*p*Phe-NCS performed equally good as DFO*-NCS in preclinical *in vivo* studies. Differences have been observed in conjugation efficiency, being less efficient for DFO-cyclo*-*p*Phe-NCS, and in lipophilicity, being higher for DFO-cyclo*-*p*Phe-NCS.[48] The fact that DFO-cyclo*-*p*Phe-NCS is a chiral compound makes this candidate less attractive from the pharmaceutical point of view. Finally, DOTA, a well-known chelator for many radiometals, has also been suggested to be able to fully coordinate and stabilize ^{89}Zr. Because of the high temperature (90 °C) needed for radiolabeling DOTA with ^{89}Zr, a prelabeling approach is required comprising the conversion of ^{89}Zr-oxalate to ^{89}Zr-chloride followed by radiolabeling of DOTA and then coupling to an antibody. However, to the best of our knowledge, ^{89}Zr-DOTA-mAb conjugates have not been evaluated *in vivo* yet.[55,56] Of note, development of novel candidate chelators for ^{89}Zr remains a very active field as exemplified by the recent introduction of oxoDFO*,[57,58] FSC derivatives,[59] 4HMS,[60] DFO2,[61] PCTA,[62] and NOTA.[62] However, for most of these chelators the suitability for stable, efficient, and inert ^{89}Zr labeling of mAbs still has to be demonstrated, while *in vivo* evaluation to prove their superiority over DFO and DFO* is lacking.

^{64}Cu. ^{64}Cu ($t_{1/2}$ = 12.7 h) is often considered a radionuclide with a short to intermediate half-life suitable for the labeling of antibody fragments with a medium to short biological half-life such as Fab and single-chain variable fragments (scFv). ^{64}Cu is generally obtained via the bombardment of enriched ^{64}Ni and provided as [^{64}Cu]$CuCl_2$. ^{64}Cu has been considered for its theranostic properties not only because of its intrinsic β^- (39.0%) emission along with its β^+ (17.9%) but also because ^{64}Cu could be used as a pair with the therapeutic β^- emitting radionuclide ^{67}Cu, although applications with the latter are still limited due to its rare and expensive production.[130] To reflect on exciting developments regarding ^{64}Cu radiopharmaceuticals, comprehensive reviews have recently been published.[9,10,22,44,130−137]

Due to the hardness of Cu^{2+} aliphatic and aromatic amines as well as carboxylates have been widely used in BFCs for antibody labeling. Cu^{2+} is capable of forming complexes with four to six coordinating ligands, of which macrocyclic chelators containing six coordinating ligands are often preferred because of their increased complex stability. Many chelators have been evaluated over the years;[19,42,44,138,139] however, DOTA remains the preferred chelator for evaluation of antibodies preclinically and clinically. This is surprising taking into account that ^{64}Cu-DOTA demonstrates far from optimal stability *in vivo* resulting in hepatobiliary excretion of released copper and its transchelation to other proteins such as superoxide dismutase. Despite its suboptimal *in vivo* performance, DOTA has the advantage that it is commercially available and can be used also for other radiometals, while it has been safely used clinically for decades.[140,141] Over the years, however, NOTA has emerged as a successful successor of DOTA in clinical studies showing improved *in vivo* stability while allowing fast (1 h or less depending on the protein) and mild labeling conditions (RT to 40 °C, pH ∼ 5−6) for heat-sensitive antibodies (see Table 2).[142] *In vivo* preclinical benchmarking studies comparing chelators are still ongoing and unsurprisingly show that DOTA is the least stable chelator for ^{64}Cu (see Table 3).

Other chelators such as various cyclams have been evaluated but do not always show superior *in vivo* stability compared to DOTA and NOTA derivatives. In addition, CB-TE2A and TETA chelators are promising but usually require radiolabeling conditions too harsh for sensitive antibodies (i.e., 90 °C), and thus their use is restricted to heat-stable proteins.[143,144] Antibodies radiolabeled with sarcophagine (Sar) derivatives have shown promising *in vivo* stability in the past with fast (20−30 min) radiolabeling at RT.[145] Research on new sarcophagine BFCs is actively ongoing and very recently showed promising results with trastuzumab.[146] Publications with antibody fragments have also been described for which in contrast to intact mAbs, kidney retention is often observed, which most probably is caused by the positive charge of the ^{64}Cu-chelator resulting in binding to negatively charged glomerulus cells in kidneys.[111]

^{68}Ga. In comparison with previously discussed radiometals such as ^{89}Zr and ^{64}Cu, ^{68}Ga emits relatively high-energy positrons ($E_{\beta max}$ = 1.9 Mev) that can hamper image quality (mean range in water 2.9 mm) (Table 1). ^{68}Ga is generally produced via the decay of its mother radionuclide Germanium-68 ($t_{1/2}$ = 271 d) and has emerged as a practical solution for small-scale PET tracer synthesis due the convenience of having a ^{68}Ge/^{68}Ga generator on site. Its short half-life ($t_{1/2}$ = 68 min) limits, however, the option of central production for multi-center applications. Nevertheless, ^{68}Ga has become a chelator of choice for radiolabeling of peptides and in recent years for antibody derivatives with a short biological half-life such as nanobodies.

$^{68}Ga^{3+}$ is considered a relatively hard cation, stable in acidic conditions, preferring hexadentate chelation via nitrogen and oxygen donors. However, $^{68}Ga^{3+}$ slowly forms insoluble $Ga(OH)_3$ complexes between pH 3 and 7, which requires complexation kinetics faster than their formation. At physiological pH, soluble $[Ga(OH)_4]^-$ is formed, which shows slow chelation kinetics. As such, radiolabeling conditions are usually chosen that prevent the formation of $Ga(OH)_3$ or in the presence of trapping reagents (i.e., citrate or acetate).[9]

Typically, ^{68}Ga is eluted from the generator as $^{68}Ga^{3+}$ in HCl solution. Over the years, many chelators have been developed, and some recent comprehensive reviews discuss in great detail the labeling conditions, yields, and variety of *in vivo* applications with ^{68}Ga-radiolabeled peptides and antibody derivatives.[9,156,157] Initially, DOTA was often used for complexation of ^{68}Ga even though high reaction temperatures were needed for good radiolabeling efficiency. However, these relatively harsh conditions are not appropriate for heat-sensitive antibodies. For this reason, the use of DOTA in preclinical (see Table 2) and clinical[158−160] studies is mainly restricted to antibodies that can handle high temperatures such as affibodies. As for ^{64}Cu, NOTA is by far the most often used

https://doi.org/10.1021/acs.bioconjchem.1c00136
Bioconjugate Chem. 2021, 32, 1315−1330

Table 3. Representative Preclinical Benchmarking Studies with ^{64}Cu Chelators Reported in the Last ~5 Years

^{64}Cu comparison of chelators	antibody derivatives	conjugation conditions	radiolabeling conditions	conclusion/comment	ref
Cu-NOTA-(NCS)/^{89}Zr-DFO-(NCS)	bivalent scFv-Fc	5 equiv; 1 h; 37 °C; pH 9.0	1 h; 37 °C; pH not indicated	Similar uptake at day 1, ^{89}Zr derivative preferred for later imaging time points (as for mAbs)	147
DOTA-(NCS)/NOTA-(NCS)	mAbs	20 equiv; 4 h; 4 °C; pH 8.5	45 min; 38 °C; pH 5	NOTA better chelator with, i.e., reduced liver uptake	148
NODAGA-(NHS)/DOTA-(NHS)	Affibodies	3–10 equiv; in DMSO, reaction quenched by TRIS pH 8 (time not indicated)	1 h; 37 °C; DOTA-affibody (pH 7.4) or NODAGA-affibody (pH 6.0)	NODAGA better chelator regarding uptake in normal organs	149
NODAGA/NOTA	Affibodies	5 equiv; overnight for NODAGA; 2 h for NOTA; RT; pH not indicated	45 min; 95 °C; pH 5.6	NODAGA complex better regarding uptake in normal organs High radiometabolites in kidneys for both tracers (usual for affibodies)	150
NODAGA(−NHS)/DOTA(−NHS)	mAb	5–100 equiv; 20 h; 4 °C; in 0.1 M borate buffered saline	30 min (DOTA) or 60 min (NODAGA); RT or 40 °C; pH 5.6	Various reaction parameters. NODAGA more stable *in vivo* than DOTA derivative, similar tumor uptake and less in normal tissues	151,152
		20 equiv; RT 3–4 h then 4 °C overnight; pH 8.3	1 h, 40 °C (DOTA-mAb) or RT (NODAGA-mAb); pH 6	Higher *in vivo* stability of NODAGA-mAb	
TE1PA-(NCS)/NOTA-(NCS)/DOTA-(NCS)/DOTA-(NHS)	mAb	20 equiv; overnight; RT; pH 8.5–8.6	30 min; 40 °C; pH 6–7	TE1PA conjugation 5 times more efficient. Better *in vivo* stability of TE1PA conjugate against DOTA regarding transchelation especially at late time points	153,154
phosphinate chelator (L5(-NCS)) compared with NODAGA-(NCS)	mAb	50 equiv; 24 h; 25 °C; pH 7.9	20 min; 37 °C; pH 5.5	Phosphinate chelator superior especially regarding uptake in normal organs	155

chelator for ^{68}Ga (Table 2).[161] NOTA has the advantage over DOTA of allowing radiolabeling at RT, and therefore is suitable for a large range of antibody derivatives.

DFO,[125] HBED,[124] and tris(hydroxypyridinone) THP[162] derivatives have also been used in recent years studies, but *in vivo* benchmarking studies proving their superiority over NOTA derivatives are still lacking even though those chelators provide attractive radiolabeling conditions.[156]

OTHER RADIONUCLIDES

^{52}Mn. ^{52}Mn is an interesting emerging radiometal for immuno-PET because of its half-life and low positron energy ($t_{1/2}$ = 5.59 d, β^+ = 29.6%, $E(\beta^+)$max = 0.576 MeV, Table 1) that offers favorable resolution for imaging (in the range of ^{18}F). There are safety concerns because of the concomitant high-energy gammas (744 keV (90%), 935 keV (95%), and 234 and 1434 keV (100%)) that result in a high radiation burden in *in vivo* applications. ^{52}Mn is commonly produced in a cyclotron via the ^{52}Cr(p,n)^{52}Mn reaction. Manganese is a hard transition metal present in solution mainly in the active oxidation states 2+ and 3+, thus offering complexation as Mn^{2+} with polyaminocarboxylic acid chelators like DOTA.

Stable Mn has been of particular interest for MRI applications with dual-modality manganese-enhanced magnetic resonance imaging (MEMRI), but despite favorable physical characteristics, its use has been limited, most probably due to the biological toxicity of bulk manganese, its accumulation in organs such as the pancreas, and its neurotoxicity that can lead to Parkinson-like impairments.[163−166] This is certainly not an issue for ^{52}Mn PET tracer applications where the amounts of Mn needed (in the nanomolar range) to obtain a PET signal are very low, thus reducing toxicity issues to the minimum.[167]

To the best of our knowledge, there is only one study that reported on the *in vivo* evaluation of a ^{52}Mn-labeled mAb. To this end, the anti-CD105 mAb TRC105 was conjugated with DOTA-NCS, followed by radiolabeling at pH 4.5 to 7.5 and a temperature ranging from RT to 55 °C. *In vivo* data showed a maximum tumor uptake of 19%ID/g 24 h p.i. of the tracer with a slow blood clearance over time and relatively high bone and spleen uptake (>10%ID/g, 120 h p.i.), which requires further investigation.[167]

^{86}Y. Yttrium-86 ($t_{1/2}$ = 14.74 h, β+ = 33%, 3.1 MeV, Table 1) has generated interest as a surrogate isotope of yttrium that could be used as a matching pair for targeted radionuclide therapy with the β^--emitter yttrium-90 ($t_{1/2}$ = 64.1 h).[168] ^{86}Y is most commonly produced via the ^{86}Sr(p,n)^{86}Y reaction. ^{86}Yttrium is a transition metal ion that prefers an octadentate coordination in its $^{86}Y^{3+}$ state and has mainly been used with the well-known polyaminocarboxylates chelators, DTPA and DOTA.[169] Just a couple of publications have described the use of ^{86}Y-DTPA radiolabeled antibodies in the last five years with successful radiolabeling under mild conditions (1 h at 37 °C in sodium acetate) including therapy studies with the corresponding ^{90}Y derivatives.[170,171] ^{86}Y presents, however, more than 65% of its decay along with γ-rays ranging from 200 to 3000 keV that hamper contrast and quantification with the presence of false coincident γ detection.

^{66}Ga. Gallium-66 ($t_{1/2}$ = 9.49 h, β+ = 56.5%, 4.2 MeV, Table 1) is another β^+-emitting isotope of gallium produced by the ^{66}Zn(p,n)^{66}Ga nuclear reaction that is envisaged as a novel tool for PET imaging and has already been applied to peptides.[172] *In vivo* applications to antibodies are, however, still

https://doi.org/10.1021/acs.bioconjchem.1c00136
Bioconjugate Chem. 2021, 32, 1315−1330

limited. An anti-EGFR affibody has been conjugated with DFO, followed by radiolabeling with ^{66}Ga, ^{68}Ga, and ^{89}Zr and their *in vivo* behavior compared. The longer half-life of ^{66}Ga allowed imaging at later time points which was beneficial for the tumor-to-organ ratios.[173] Although ^{66}Ga seems to be a more interesting radionuclide than ^{68}Ga for the labeling of antibody derivatives with a longer serum half-life, application is limited due to its high positron range (R_{mean} = 9.3 mm in water) and co-emitting gammas that hamper spatial resolution and reliable PET quantification.[174]

^{44}Sc. ^{44}Sc can be obtained via a ^{44}Ti/^{44}Sc generator or via production in a cyclotron using a ^{44}Ca(p,n)^{44}Sc reaction (see Table 1). Thus far, focus has been on improving the ^{44}Sc production process to reduce costs that has been limiting its applicability.[9,175−179] A half-life of about 4 h and a decay to nontoxic Ca make ^{44}Sc an interesting radionuclide for immuno-PET imaging. Scandium is present in aqueous solutions as the hard trivalent cation Sc^{3+} with a strong preference for hard oxygen donor ligands and a flexible coordination number (between 3 and 9, with 6 being the most reported).[180] ^{44}Sc complexation strongly depends on pH, with pH 4 being considered the most optimal for radiolabeling.[180] ^{44}Sc is a PET radionuclide with growing interest in recent years, however, mostly in the field of peptide labeling. This is probably due to the relatively harsh radiolabeling conditions not being compatible with antibodies. To date, first in human studies have been reported with peptides (i.e., PSMA and DOTATOC) but not with larger biomolecules.[181] Moreover, ^{44}Sc is considered to form a theranostic pair with the therapeutic radionuclides ^{177}Lu ($t_{1/2}$ = 6.7 days) and ^{47}Sc ($t_{1/2}$ = 3.4 days), although their half-lives do not match optimally.[182]

Various chelators have been tested for ^{44}Sc, with DOTA being favorable, but its application is still restricted to affibodies which can handle the required high reaction temperatures of 90−110 °C.[183,184] Other chelators include a DTPA derivative, which was coupled to a Fab fragment of cetuximab and further evaluated *in vivo*. Radiolabeling was fast (30 min) at RT and gave better yields than the DOTA and NOTA derivatives.[185] Finally, H_3 mpatcn (see Figure 2), a small triazamacrocyclic picolinate-functionalized chelator, showed efficient labeling of peptides at RT, but does not seem to have been applied to antibody derivatives yet.[186] Of note, uncoupled Sc as in Sc(III)-citrate has been found to accumulate in liver, spleen, and bone with possible accumulation of colloids in lungs and heart.[180]

^{18}F in [^{18}F]AlF. In this review on radiometals for immuno-PET, it appears relevant to also discuss the progress on labeling of antibodies with ^{18}F via aluminum. ^{18}F is by far the most often used PET radionuclide for small molecule imaging thanks to its short half-life (110 min) and ideal physical properties ($E_{\beta max}$ = 0.6 MeV, mean range in water = 0.6 mm). Labeling procedures with ^{18}F can, however, be time-consuming and harsh with multiple drying and purification steps that decrease overall yields significantly, while the use of organic solvents and high-temperature conditions are not compatible with antibodies. As fluorine is able to form strong bonds with metals, especially aluminum,[187] [^{18}F]AlF radiochemistry is opening new possibilities for fast metal complexation and thus radiolabeling of antibodies.[188−191]

^{18}F is easily available via commercial suppliers and produced in a cyclotron via the ^{18}O(p,n)^{18}F nuclear reaction. $AlCl_3$ is used to prepare a stock solution of Al^{3+} in typically 0.1 M sodium acetate at pH ∼ 4 to which fluorine is further added and incubated to form a strong [^{18}F]AlF bond followed by purification, for example, over a QMA cartridge to remove free ^{18}F and other metal contaminants.[192] Radiolabeling of NOTA and NODA derivatives with [^{18}F]AlF is done at high temperature (100−110 °C) in a short reaction time (15 min) and results in very stable complexes. However, the high radiolabeling temperature has prevented direct labeling of heat-sensitive antibodies.[193−196] One of the most promising developments in this field is the development of the acyclic pentadentate chelator (±)-H3RESCA which possesses a N_2O_3 coordinating set of donor atoms, which can strongly complex [^{18}F]AlF at room temperature for which Cleeren et al.[197] filed a patent in 2016.[198,199]

Twelve-to-fifteen times excess of the chelator (±)-H3RESCA, a pentadentate ligand with N_2O_3 donor groups, is typically reacted with the antibody derivative (i.e., a nanobody) in aqueous solution and incubation for 2−3 h at RT and at pH 8.5−8.7 resulting in a chelator-to-protein ratio between 1 and 2.[198] Radiolabeling is performed under mild conditions (pH 4−5, RT to 37 °C, 12−15 min, see Table 2), and a cosolvent (i.e., ethanol) is generally used to increase radiolabeling yields.

^{18}F-labeling of antibodies via this chelator has, however, raised a few points of concern. Elevated bone uptake has been observed indicating demetalation and/or defluorination and seems to depend on the pharmacokinetics of the molecule itself but could also be animal-species-dependent.[198] The assumed mechanism of *in vivo* degradation involves glomerular filtration and conjugate degradation resulting in release and recirculation of free ^{18}F. This phenomenon might also be dependent on the biological molecule itself, its half-life, preference for renal excretion, and the preclinical model used. Furthermore, the slightly more lipophilic nature of (±)-H3RESCA in comparison with other chelators such as NOTA could induce increased hepatic clearance.[198] *In vivo* preclinical and clinical studies should confirm the potential of (±)-H3RESCA for [^{18}F]AlF radiolabeling of antibodies.

CONCLUSION

Radiolabeling of antibodies with radiometals is a growing and exciting field within PET imaging for which tremendous efforts have been made to develop general conjugation and radiolabeling methods with chelators that could be used for multiple radiometals. As illustrated in this review, there is, however, still no ideal chelator that could be used in an optimal way for multiple radiometals and compromises have to be made between ideal and practical aspects. Ideally, such a chelator should be commercially available and able to complex in a stable way multiple radiometals following well-established procedures and without altering the properties of the antibody to boost clinical applications. This remains, however, a challenge for the future of immuno-PET, as each radiometal possesses its own chemical and (sometimes harsh) labeling properties along with its specific decay characteristics. Bioconjugation and radiolabeling procedures should furthermore be GMP-compliant to facilitate translation to the clinic. Production costs and availability of the radiometal, the quality and *in vivo* performance of the obtained radioimmunoconjugate, and the logistics of its production and distribution are thus primordial parameters to take into account. For those reasons, despite very active developments in preclinical studies, the commercially available chelators, DFO, DOTA, and

https://doi.org/10.1021/acs.bioconjchem.1c00136
Bioconjugate Chem. 2021, 32, 1315−1330

NOTA, are still by far the most often used chelators in the clinic. Among the other promising radiometal−chelator pairs discussed in this review, future preclinical and clinical studies will confirm their potential as new gold standards for immuno-PET imaging.

AUTHOR INFORMATION

Corresponding Author

Danielle J. Vugts − *Amsterdam UMC, Vrije Universiteit Amsterdam, Radiology & Nuclear Medicine, Cancer Center Amsterdam, Amsterdam 1081 HV, The Netherlands*; Email: d.vugts@amsterdamumc.nl

Authors

Marion Chomet − *Amsterdam UMC, Vrije Universiteit Amsterdam, Radiology & Nuclear Medicine, Cancer Center Amsterdam, Amsterdam 1081 HV, The Netherlands*; orcid.org/0000-0001-9632-4875

Guus A. M. S. van Dongen − *Amsterdam UMC, Vrije Universiteit Amsterdam, Radiology & Nuclear Medicine, Cancer Center Amsterdam, Amsterdam 1081 HV, The Netherlands*

Complete contact information is available at: https://pubs.acs.org/10.1021/acs.bioconjchem.1c00136

Notes

The authors declare no competing financial interest.

REFERENCES

(1) Vugts, D. J., and van Dongen, G. A. M. S. (2019) Immunoglobulins as Radiopharmaceutical Vectors. In *Radiopharmaceutical Chemistry* (Lewis, J. S., Windhorst, A. D., and Zeglis, B. M., Eds.) pp 163−179, Springer International Publishing, Cham. DOI: 10.1007/978-3-319-98947-1_9.

(2) van Dongen, G. A. M. S., Beaino, W., Windhorst, A. D., Zwezerijnen, G. J. C., Oprea-Lager, D. E., Hendrikse, N. H., van Kuijk, C., Boellaard, R., Huisman, M. C., and Vugts, D. J. (2021) The Role of 89Zr-Immuno-PET in Navigating and Derisking the Development of Biopharmaceuticals. *J. Nucl. Med. 62* (4), 438−445.

(3) Lambert, J. M., and Morris, C. Q. (2017) Antibody-Drug Conjugates (ADCs) for Personalized Treatment of Solid Tumors: A Review. *Adv. Ther. 34* (5), 1015−1035.

(4) Bouchard, H., Viskov, C., and Garcia-Echeverria, C. (2014) Antibody-Drug Conjugates—A New Wave of Cancer Drugs. *Bioorg. Med. Chem. Lett. 24* (23), 5357−5363.

(5) Singh, S., Kumar, N. K., Dwiwedi, P., Charan, J., Kaur, R., Sidhu, P., and Chugh, V. K. (2018) Monoclonal Antibodies: A Review. *Curr. Clin. Pharmacol. 13* (2), 85−99.

(6) Kaplon, H., Muralidharan, M., Schneider, Z., and Reichert, J. M. (2020) Antibodies to Watch in 2020. *MAbs 12* (1), 1703531.

(7) Lu, R. M., Hwang, Y. C., Liu, I. J., Lee, C. C., Tsai, H. Z., Li, H. J., and Wu, H. C. (2020) Development of Therapeutic Antibodies for the Treatment of Diseases. *J. Biomed. Sci. 27* (1), 1−30.

(8) Zanzonico, P. (2019) An Overview of Nuclear Imaging. In *Radiopharmaceutical Chemistry*, pp 101−117, Springer International Publishing, Cham. DOI: 10.1007/978-3-319-98947-1_6.

(9) Price, T. W., Greenman, J., and Stasiuk, G. J. (2016) Current Advances in Ligand Design for Inorganic Positron Emission Tomography Tracers 68Ga, 64Cu, 89Zr and 44Sc. *Dalt. Trans. 45* (40), 15702−15724.

(10) Boros, E., and Holland, J. P. (2018) Chemical Aspects of Metal Ion Chelation in the Synthesis and Application Antibody-Based Radiotracers. *J. Labelled Compd. Radiopharm. 61* (9), 652−671.

(11) Verel, I., Visser, G. W. M., Boellaard, R., Boerman, O. C., van Eerd, J., Snow, G. B., Lammertsma, A. A., and van Dongen, G. A. M. S. (2003) Quantitative 89Zr Immuno-PET for in Vivo Scouting of 90Y-Labeled Monoclonal Antibodies in Xenograft-Bearing Nude Mice. *J. Nucl. Med. 44* (10), 1663−1670.

(12) Filippi, L., Chiaravalloti, A., Schillaci, O., Cianni, R., and Bagni, O. (2020) Theranostic Approaches in Nuclear Medicine: Current Status and Future Prospects. *Expert Rev. Med. Devices 17* (4), 331−343.

(13) Notni, J., and Wester, H. J. (2018) Re-Thinking the Role of Radiometal Isotopes: Towards a Future Concept for Theranostic Radiopharmaceuticals. *J. Labelled Compd. Radiopharm. 61* (3), 141−153.

(14) Zeglis, B. M., and Lewis, J. S. (2011) A Practical Guide to the Construction of Radiometallated Bioconjugates for Positron Emission Tomography. *Dalt. Trans 40* (23), 6168−6195.

(15) Morais, M., Ma, M. T., and Chudasama, V. (2018) Site-Specific Chelator-Antibody Conjugation for PET and SPECT Imaging with Radiometals. *Drug Discovery Today: Technol. 30*, 91−104.

(16) Adumeau, P., Sharma, S. K., Brent, C., and Zeglis, B. M. (2016) Site-Specifically Labeled Immunoconjugates for Molecular Imaging—Part 1: Cysteine Residues and Glycans. *Mol. Imaging Biol. 18* (1), 1−17.

(17) Adumeau, P., Kiran Sharma, S., Brent, C., and Zeglis, B. M. (2016) Site-Specifically Labeled Immunoconjugates for Molecular Imaging-Part 2: Peptide Tags and Unnatural Amino Acids HHS Public Access. *Mol. Imaging Biol. 18* (2), 153−165.

(18) Meyer, J.-P., Adumeau, P., Lewis, J. S., and Zeglis, B. M. (2016) Click Chemistry and Radiochemistry: The First 10 Years Graphical Abstract HHS Public Access. *Bioconjugate Chem. 27* (12), 2791−2807.

(19) Wei, W., Rosenkrans, Z. T., Liu, J., Huang, G., Luo, Q.-Y., and Cai, W. (2020) ImmunoPET: Concept, Design, and Applications. *Chem. Rev. 120* (8), 3787−3851.

(20) Lindmo, T., Boven, E., Cuttitta, F., Fedorko, J., and Bunn, P. A. (1984) Determination of the Immunoreactive Function of Radiolabeled Monoclonal Antibodies by Linear Extrapolation to Binding at Infinite Antigen Excess. *J. Immunol. Methods 72* (1), 77−89.

(21) de Vries, E. G. E., Kist de Ruijter, L., Lub-De Hooge, M. N., Dierckx, R. A., Elias, S. G., and Oosting, S. F. (2019) Integrating Molecular Nuclear Imaging in Clinical Research to Improve Anticancer Therapy. *Nat. Rev. Clin. Oncol. 16* (4), 241−255.

(22) Aluicio-Sarduy, E., Ellison, P. A., Barnhart, T. E., Cai, W., Nickles, R. J., and Engle, J. W. (2018) PET Radiometals for Antibody Labeling. *J. Labelled Compd. Radiopharm. 61* (9), 636−651.

(23) Verel, I., Visser, G. W. M., Boellaard, R., Walsum, M. S., Van Snow, G. B., and Van Dongen, G. A. M. S. (2003) 89Zr Immuno-PET: Comprehensive Procedures for the Production of 89Zr-Labeled Monoclonal Antibodies. *J. Nucl. Med. 44* (8), 1271−1281.

(24) Perk, L. R., Vosjan, M. J. W. D., Visser, G. W. M., Budde, M., Jurek, P., Kiefer, G. E., and van Dongen, G. A. M. S. (2010) P-Isothiocyanatobenzyl-Desferrioxamine: A New Bifunctional Chelate for Facile Radiolabeling of Monoclonal Antibodies with Zirconium-89 for Immuno-PET Imaging. *Eur. J. Nucl. Med. Mol. Imaging 37* (2), 250−259.

(25) Zeglis, B. M., and Lewis, J. S. (2015) The Bioconjugation and Radiosynthesis of ^{89}Zr-DFO-Labeled Antibodies. *J. Visualized Exp.*, 96.

(26) Sharma, S. K., Glaser, J. M., Edwards, K. J., Khozeimeh Sarbisheh, E., Salih, A. K., Lewis, J. S., and Price, E. W. (2020) A Systematic Evaluation of Antibody Modification and 89Zr-Radiolabeling for Optimized Immuno-PET. *Bioconjugate Chem.*, 1 DOI: 10.1021/acs.bioconjchem.0c00087.

(27) Vosjan, M. J. W. D., Perk, L. R., Visser, G. W. M., Budde, M., Jurek, P., Kiefer, G. E., and van Dongen, G. A. M. S. (2010) Conjugation and Radiolabeling of Monoclonal Antibodies with Zirconium-89 for PET Imaging Using the Bifunctional Chelate p-Isothiocyanatobenzyl-Desferrioxamine. *Nat. Protoc. 5* (4), 739−743.

(28) Cohen, R., Stammes, M. A., de Roos, I. H., Stigter-Van Walsum, M., Visser, G. W., and van Dongen, G. A. (2011) Inert Coupling of IRDye800CW to Monoclonal Antibodies for Clinical Optical Imaging of Tumor Targets. *EJNMMI Res. 1* (1), 31.

(29) Wei, W., Rosenkrans, Z. T., Liu, J., Huang, G., Luo, Q. Y., and Cai, W. (2020) ImmunoPET: Concept, Design, and Applications. *Chem. Rev. 120*, 3787−3851.
(30) Yoon, J.-K., Park, B.-N., Ryu, E.-K., An, Y.-S., and Lee, S.-J. (2020) Current Perspectives on 89Zr-PET Imaging. *Int. J. Mol. Sci. 21* (12), 4309.
(31) Guérard, F., Lee, Y.-S., Tripier, R., Szajek, L. P., Deschamps, J. R., and Brechbiel, M. W. (2013) Investigation of Zr(IV) and 89Zr(IV) Complexation with Hydroxamates: Progress towards Designing a Better Chelator than Desferrioxamine B for Immuno-PET Imaging. *Chem. Commun. 49* (10), 1002−1004.
(32) Holland, J. P., and Vasdev, N. (2014) Charting the Mechanism and Reactivity of Zirconium Oxalate with Hydroxamate Ligands Using Density Functional Theory: Implications in New Chelate Design. *Dalt. Trans. 43* (26), 9872−9884.
(33) Wadas, T. J., Wong, E. H., Weisman, G. R., and Anderson, C. J. (2010) Coordinating Radiometals of Copper, Gallium, Indium, Yttrium, and Zirconium for PET and SPECT Imaging of Disease. *Chem. Rev. 110* (5), 2858−2902.
(34) Holland, J. P., Divilov, V., Bander, N. H., Smith-Jones, P. M., Larson, S. M., and Lewis, J. S. (2010) 89Zr-DFO-J591 for ImmunoPET of Prostate-Specific Membrane Antigen Expression In Vivo. *J. Nucl. Med. 51* (8), 1293−1300.
(35) Abou, D. S., Ku, T., and Smith-Jones, P. M. (2011) In Vivo Biodistribution and Accumulation of 89Zr in Mice. *Nucl. Med. Biol. 38* (5), 675−681.
(36) Severin, G. W., Jørgensen, J. T., Wiehr, S., Rolle, A.-M., Hansen, A. E., Maurer, A., Hasenberg, M., Pichler, B., Kjær, A., and Jensen, A. I. (2015) The Impact of Weakly Bound 89Zr on Preclinical Studies: Non-Specific Accumulation in Solid Tumors and Aspergillus Infection. *Nucl. Med. Biol. 42* (4), 360−368.
(37) Deri, M. A., Ponnala, S., Kozlowski, P., Burton-Pye, B. P., Cicek, H. T., Hu, C., Lewis, J. S., and Francesconi, L. C. (2015) p-SCN-Bn-HOPO: A Superior Bifunctional Chelator for 89Zr ImmunoPET. *Bioconjugate Chem. 26* (12), 2579−2591.
(38) Fischer, G., Seibold, U., Schirrmacher, R., Wängler, B., and Wängler, C. (2013) 89Zr, a Radiometal Nuclide with High Potential for Molecular Imaging with PET: Chemistry, Applications and Remaining Challenges. *Molecules 18* (6), 6469−6490.
(39) Heskamp, S., Raavé, R., Boerman, O., Rijpkema, M., Goncalves, V., and Denat, F. (2017) 89Zr-Immuno-Positron Emission Tomography in Oncology: State-of-the-Art 89Zr Radiochemistry. *Bioconjugate Chem. 28* (9), 2211−2223.
(40) Bhatt, N., Pandya, D., and Wadas, T. (2018) Recent Advances in Zirconium-89 Chelator Development. *Molecules 23* (3), 638.
(41) Deri, M. A., Zeglis, B. M., Francesconi, L. C., and Lewis, J. S. (2013) PET Imaging with ^{89}Zr: From Radiochemistry to the Clinic. *Nucl. Med. Biol. 40* (1), 3−14.
(42) Brandt, M., Cardinale, J., Aulsebrook, M. L., Gasser, G., and Mindt, T. L. (2018) An Overview of PET Radiochemistry, Part 2: Radiometals. *J. Nucl. Med. 59* (10), 1500−1506.
(43) Dilworth, J. R., and Pascu, S. I. (2018) The Chemistry of PET Imaging with Zirconium-89. *Chem. Soc. Rev. 47* (8), 2554−2571.
(44) Boros, E., and Packard, A. B. (2019) Radioactive Transition Metals for Imaging and Therapy. *Chem. Rev. 119* (2), 870−901.
(45) La, M. T., Tran, V. H., and Kim, H.-K. (2019) Progress of Coordination and Utilization of Zirconium-89 for Positron Emission Tomography (PET) Studies. *Nucl. Med. Mol. Imaging 53* (2), 115−124.
(46) Patra, M., Bauman, A., Mari, C., Fischer, C. A., Blacque, O., Häussinger, D., Gasser, G., Mindt, T. L., Fischer, G., Seibold, U., et al. (2014) An Octadentate Bifunctional Chelating Agent for the Development of Stable Zirconium-89 Based Molecular Imaging Probes. *Chem. Commun. 50* (78), 11523−11525.
(47) Vugts, D. J., Klaver, C., Sewing, C., Poot, A. J., Adamzek, K., Huegli, S., Mari, C., Visser, G. W. M., Valverde, I. E., Gasser, G., et al. (2017) Comparison of the Octadentate Bifunctional Chelator DFO*-PPhe-NCS and the Clinically Used Hexadentate Bifunctional Chelator DFO-PPhe-NCS for 89Zr-Immuno-PET. *Eur. J. Nucl. Med. Mol. Imaging 44* (2), 286−295.
(48) Raavé, R., Sandker, G., Adumeau, P., Jacobsen, C. B., Mangin, F., Meyer, M., Moreau, M., Bernhard, C., Da Costa, L., Dubois, A., et al. (2019) Direct Comparison of the in Vitro and in Vivo Stability of DFO, DFO* and DFOcyclo* for 89Zr-ImmunoPET. *Eur. J. Nucl. Med. Mol. Imaging 46* (9), 1966−1977.
(49) Cho, H., Al-Saden, N., Lam, H., Möbus, J., Reilly, R. M., and Winnik, M. A. (2020) A Comparison of DFO and DFO* Conjugated to Trastuzumab-DM1 for Complexing 89Zr - In Vitro Stability and in Vivo MicroPET/CT Imaging Studies in NOD/SCID Mice with HER2-Positive SK-OV-3 Human Ovarian Cancer Xenografts. *Nucl. Med. Biol. 84−85*, 11−19.
(50) Chomet, M., Schreurs, M., Bolijn, M. J., Verlaan, M., Beaino, W., Brown, K., Poot, A. J., Windhorst, A. D., Gill, H., Marik, J., et al. (2021) Head-to-Head Comparison of DFO* and DFO Chelators: Selection of the Best Candidate for Clinical 89Zr-Immuno-PET. *Eur. J. Nucl. Med. Mol. Imaging 48* (3), 694−707.
(51) Berg, E., Gill, H., Marik, J., Ogasawara, A., Williams, S., van Dongen, G., Vugts, D., Cherry, S. R., and Tarantal, A. F. (2020) Total-Body PET and Highly Stable Chelators Together Enable Meaningful 89Zr-Antibody PET Studies up to 30 Days After Injection. *J. Nucl. Med. 61* (3), 453−460.
(52) Rudd, S. E., Roselt, P., Cullinane, C., Hicks, R. J., and Donnelly, P. S. (2016) A Desferrioxamine B Squaramide Ester for the Incorporation of Zirconium-89 into Antibodies. *Chem. Commun. 52* (80), 11889−11892.
(53) Holland, J. P. (2020) Predicting the Thermodynamic Stability of Zirconium Radiotracers. *Inorg. Chem. 59* (3), 2070−2082.
(54) Bhupathiraju, N. V. S. D. K., Younes, A., Cao, M., Ali, J., Cicek, H. T., Tully, K. M., Ponnala, S., Babich, J. W., Deri, M. A., Lewis, J. S., et al. (2019) Improved Synthesis of the Bifunctional Chelator p-SCN-Bn-HOPO. *Org. Biomol. Chem. 17* (28), 6866−6871.
(55) Pandya, D. N., Bhatt, N., Yuan, H., Day, C. S., Ehrmann, B. M., Wright, M., Bierbach, U., and Wadas, T. J. (2017) Zirconium Tetraazamacrocycle Complexes Display Extraordinary Stability and Provide a New Strategy for Zirconium-89-Based Radiopharmaceutical Development. *Chem. Sci. 8* (3), 2309−2314.
(56) Pandya, D. N., Bhatt, N. B., Almaguel, F., Rideout-Danner, S., Gage, H. D., Solingapuram Sai, K. K., and Wadas, T. J. (2019) 89 Zr-Chloride Can Be Used for Immuno-PET Radiochemistry Without Loss of Antigen Reactivity In Vivo. *J. Nucl. Med. 60* (5), 696−701.
(57) Briand, M., Aulsebrook, M. L., Mindt, T. L., and Gasser, G. (2017) A Solid Phase-Assisted Approach for the Facile Synthesis of a Highly Water-Soluble Zirconium-89 Chelator for Radiopharmaceutical Development. *Dalt. Trans. 46* (47), 16387−16389.
(58) Brandt, M., Cowell, J., Aulsebrook, M. L., Gasser, G., and Mindt, T. L. (2020) Radiolabelling of the Octadentate Chelators DFO* and OxoDFO* with Zirconium-89 and Gallium-68. *JBIC, J. Biol. Inorg. Chem. 25* (5), 789−796.
(59) Zhai, C., He, S., Ye, Y., Rangger, C., Kaeopookum, P., Summer, D., Haas, H., Kremser, L., Lindner, H., and Foster, J. (2019) Rational Design, Synthesis and Preliminary Evaluation of Novel Fusarinine C-Based Chelators for Radiolabeling with Zirconium-89. *Biomolecules 9* (3), 91.
(60) Alnahwi, A. H., Ait-Mohand, S., Dumulon-Perreault, V., Dory, Y. L., and Guérin, B. (2020) Promising Performance of 4HMS, a New Zirconium-89 Octadendate Chelator. *ACS Omega 5* (19), 10731−10739.
(61) Sarbisheh, E. K., Salih, A. K., Raheem, S. J., Lewis, J. S., and Price, E. W. (2020) A High-Denticity Chelator Based on Desferrioxamine for Enhanced Coordination of Zirconium-89. *Inorg. Chem. 59* (16), 11715−11727.
(62) Pandya, D. N., Henry, K. E., Day, C. S., Graves, S. A., Nagle, V. L., Dilling, T. R., Sinha, A., Ehrmann, B. M., Bhatt, N. B., Menda, Y., et al. (2020) Polyazamacrocycle Ligands Facilitate 89Zr Radiochemistry and Yield 89Zr Complexes with Remarkable Stability. *Inorg. Chem. 59* (23), 17473−17487.

https://doi.org/10.1021/acs.bioconjchem.1c00136
Bioconjugate Chem. 2021, 32, 1315−1330

(63) Poot, A. J., Adamzek, K. W. A., Windhorst, A. D., Vosjan, M. J. W. D., Kropf, S., Wester, H.-J., van Dongen, G. A. M. S., and Vugts, D. J. (2019) Fully Automated 89Zr Labeling and Purification of Antibodies. *J. Nucl. Med. 60* (5), 691−695.
(64) Jung, K.-H., Park, J. W., Lee, J. H., Lee, E. J., Moon, S. H., Cho, Y. S., and Lee, K.-H. (2020) 89Zr Labeled Anti-PD-L1 Antibody PET Monitors Gemcitabine Therapy-Induced Modulation of Tumor PD-L1 Expression. *J. Nucl. Med.*, 250720.
(65) Martins, C. D., Da Pieve, C., Burley, T. A., Smith, R., Ciobota, D. M., Allott, L., Harrington, K. J., Oyen, W. J. G., Smith, G., and Kramer-Marek, G. (2018) HER3-Mediated Resistance to Hsp90 Inhibition Detected in Breast Cancer Xenografts by Affibody-Based PET Imaging. *Clin. Cancer Res. 24* (8), 1853−1865.
(66) Sijbrandi, N. J., Merkul, E., Muns, J. A., Waalboer, D. C. J., Adamzek, K., Bolijn, M., Montserrat, V., Somsen, G. W., Haselberg, R., Steverink, P. J. G. M., et al. (2017) A Novel Platinum(II)-Based Bifunctional ADC Linker Benchmarked Using 89Zr-Desferal and Auristatin F-Conjugated Trastuzumab. *Cancer Res. 77* (2), 257−267.
(67) Li, W., Wang, Y., Rubins, D., Bennacef, I., Holahan, M., Haley, H., Purcell, M., Gantert, L., Hseih, S., Judo, M., et al. (2021) PET/CT Imaging of 89Zr-N-SucDf-Pembrolizumab in Healthy Cynomolgus Monkeys. *Mol. Imaging Biol. 23* (2), 250−259.
(68) Liapis, V., Tieu, W., Rudd, S. E., Donnelly, P. S., Wittwer, N. L., Brown, M. P., and Staudacher, A. H. (2020) Improved Non-Invasive Positron Emission Tomographic Imaging of Chemotherapy-Induced Tumor Cell Death Using Zirconium-89-Labeled APOMAB®. *EJNMMI Radiopharm. Chem. 5* (1), 1 DOI: 10.1186/s41181-020-00109-6.
(69) Qi, S., Hoppmann, S., Xu, Y., and Cheng, Z. (2019) PET Imaging of HER2-Positive Tumors with Cu-64-Labeled Affibody Molecules. *Mol. Imaging Biol. 21*, 907−916.
(70) Yamaguchi, A., Achmad, A., Hanaoka, H., Heryanto, Y. D., Bhattarai, A., Ratianto Khongorzul, E., Shintawati, R., Kartamihardja, A. A. P., Kanai, A., et al. (2019) Immuno-PET Imaging for Non-Invasive Assessment of Cetuximab Accumulation in Non-Small Cell Lung Cancer. *BMC Cancer 19* (1), 1000.
(71) Natarajan, A., Mayer, A. T., Reeves, R. E., Nagamine, C. M., and Gambhir, S. S. (2017) Development of a Novel ImmunoPET Tracer to Image Human PD-1 Checkpoint Expression on Tumor Infiltrating Lymphocytes in a Humanized Mouse Model HHS Public Access. *Mol. Imaging Biol. 19* (6), 903−914.
(72) Srideshikan, S. M., Brooks, J., Zuro, D., Kumar, B., Sanchez, J., Echavarria Parra, L., Orellana, M., Vishwasrao, P., Nair, I., Chea, J., et al. (2019) ImmunoPET, [64Cu]Cu-DOTA-Anti-CD33 PET-CT, Imaging of an AML Xenograft Model. *Clin. Cancer Res. 25* (24), 7463−7474.
(73) Ehlerding, E. B., England, C. G., Majewski, R. L., Valdovinos, H. F., Jiang, D., Liu, G., Mcneel, D. G., Nickles, R. J., and Cai, W. (2017) ImmunoPET Imaging of CTLA-4 Expression in Mouse Models of Non-Small Cell Lung Cancer Graphical Abstract HHS Public Access. *Mol. Pharmaceutics 14* (5), 1782−1789.
(74) Woo, S.-K., Jang, S. J., Seo, M.-J., Park, J. H., Kim, B. S., Kim, E. J., Lee, Y. J., Lee, T. S., An, G. Il, Song, I. H., et al. (2019) Development of 64Cu-NOTA-Trastuzumab for HER2 Targeting: A Radiopharmaceutical with Improved Pharmacokinetics for Human Studies. *J. Nucl. Med. 60* (1), 26−33.
(75) Luo, H., England, C. G., Graves, S. A., Sun, H., Liu, G., Nickles, R. J., and Cai, W. (2016) PET Imaging of VEGFR-2 Expression in Lung Cancer with 64Cu-Labeled Ramucirumab. *J. Nucl. Med. 57* (2), 285−290.
(76) Wei, W., Jiang, D., Lee, H. J., Li, M., Kutyreff, C. J., Engle, J. W., Liu, J., and Cai, W. (2020) Development and Characterization of CD54-Targeted ImmunoPET Imaging in Solid Tumors. *Eur. J. Nucl. Med. Mol. Imaging 47* (12), 2765−2775.
(77) Song, I. H., Jeong, M. S., Hong, H. J., Shin, J. Il, Park, Y. S., Woo, S. K., Moon, B. S., Kim, K. Il, Lee, Y. J., Kang, J. H., et al. (2019) Development of a Theranostic Convergence Bioradiopharmaceutical for Immuno-PET Based Radioimmunotherapy of L1CAM in Cholangiocarcinoma Model. *Clin. Cancer Res. 25* (20), 6148−6159.
(78) Wei, W., Liu, Q., Jiang, D., Zhao, H., Kutyreff, C. J., Engle, J. W., Liu, J., and Cai, W. (2020) Tissue Factor-Targeted ImmunoPET Imaging and Radioimmunotherapy of Anaplastic Thyroid Cancer. *Adv. Sci. 7* (13), 1903595.
(79) Paquette, M., Vilera-Perez, L. G., Beaudoin, S., Ekindi-Ndongo, N., Boudreaut, P. L., Bonin, M. A., Battista, M. C., Bentourkia, M., Lopez, A. F., Lecomte, R., et al. (2017) Targeting IL-5Rα with Antibody-Conjugates Reveals a Strategy for Imaging and Therapy for Invasive Bladder Cancer. *Oncoimmunology 6* (10), 1331195.
(80) Hoffmann, S. H. L., Reck, D. I., Maurer, A., Fehrenbacher, B., Sceneay, J. E., Poxleitner, M., Öz, H. H., Ehrlichmann, W., Reischl, G., Fuchs, K., et al. (2019) Visualization and Quantification of in Vivo Homing Kinetics of Myeloid-Derived Suppressor Cells in Primary and Metastatic Cancer. *Theranostics 9* (20), 5869−5885.
(81) Kristensen, L. K., Christensen, C., Alfsen, M. Z., Cold, S., Nielsen, C. H., and Kjaer, A. (2020) Monitoring CD8a+ T Cell Responses to Radiotherapy and CTLA-4 Blockade Using [64Cu]-NOTA-CD8a PET Imaging. *Mol. Imaging Biol. 22* (4), 1021−1030.
(82) Shi, S., Hong, H., Orbay, H., Graves, S. A., Yang, Y., Ohman, J. D., Liu, B., Nickles, R. J., Wong, H. C., and Cai, W. (2015) ImmunoPET of Tissue Factor Expression in Triple-Negative Breast Cancer with a Radiolabeled Antibody Fab Fragment. *Eur. J. Nucl. Med. Mol. Imaging 42* (8), 1295−1303.
(83) Shi, S., Orbay, H., Yang, Y., Graves, S. A., Nayak, T. R., Hong, H., Hernandez, R., Luo, H., Goel, S., Theuer, C. P., et al. (2015) PET Imaging of Abdominal Aortic Aneurysm with 64Cu-Labeled Anti-CD105 Antibody Fab Fragment. *J. Nucl. Med. 56* (6), 927−932.
(84) Ehlerding, E. B., Lee, H. J., Jiang, D., Ferreira, C. A., Zahm, C. D., Huang, P., Engle, J. W., Mcneel, D. G., and Cai, W. (2019) Antibody and Fragment-Based PET Imaging of CTLA-4+ T-Cells in Humanized Mouse Models. *Am. J. Cancer Res. 9* (1), 53−63.
(85) Boyle, A. J., Cao, P.-J., Hedley, D. W., Sidhu, S. S., Winnik, M. A., and Reilly, R. M. (2015) MicroPET/CT Imaging of Patient-Derived Pancreatic Cancer Xenografts Implanted Subcutaneously or Orthotopically in NOD-Scid Mice Using 64Cu-NOTA-Panitumumab F(Ab')2 Fragments. *Nucl. Med. Biol. 42* (2), 71−77.
(86) Sun, H., England, C. G., Hernandez, R., Graves, S. A., Majewski, R. L., Kamkaew, A., Jiang, D., Barnhart, T. E., Yang, Y., and Cai, W. (2016) ImmunoPET for Assessing the Differential Uptake of a CD146-Specific Monoclonal Antibody in Lung Cancer. *Eur. J. Nucl. Med. Mol. Imaging 43* (12), 2169−2179.
(87) Lam, K., Chan, C., and Reilly, R. M. (2017) Development and Preclinical Studies of 64Cu-NOTA-Pertuzumab F(Ab′) 2 for Imaging Changes in Tumor HER2 Expression Associated with Response to Trastuzumab by PET/CT. *MAbs 9* (1), 154−164.
(88) Luo, H., England, C. G., Shi, S., Graves, S. A., Hernandez, R., Liu, B., Theuer, C. P., Wong, H. C., Nickles, R. J., and Cai, W. (2016) Dual Targeting of Tissue Factor and CD105 for Preclinical PET Imaging of Pancreatic Cancer. *Clin. Cancer Res. 22* (15), 3821−3830.
(89) Kim, H.-Y., Wang, X., Kang, R., Tang, D., Boone, B. A., Zeh, H. J., Lotze, M. T., and Edwards, W. B. (2018) RAGE-Specific Single Chain Fv for PET Imaging of Pancreatic Cancer. *PLoS One 13* (3), No. e0192821.
(90) Luo, H., England, C. G., Goel, S., Graves, S. A., Ai, F., Liu, B., Theuer β, C. P., Wong, H. C., Nickles, R. J., and Cai, W. (2017) ImmunoPET and Near-Infrared Fluorescence Imaging of Pancreatic Cancer with a Dual-Labeled Bispecific Antibody Fragment HHS Public Access. *Mol. Pharmaceutics 14* (5), 1646−1655.
(91) White, J. B., Hu, L. Y., Boucher, D. L., and Sutcliffe, J. L. (2018) ImmunoPET Imaging of Avβ6 Expression Using an Engineered Anti-Avβ6 Cys-Diabody Site-Specifically Radiolabeled with Cu-64: Considerations for Optimal Imaging with Antibody Fragments. *Mol. Imaging Biol. 20* (1), 103−113.
(92) Senders, M. L., Hernot, S., Carlucci, G., van de Voort, J. C., Fay, F., Calcagno, C., Tang, J., Alaarg, A., Zhao, Y., Ishino, S., et al. (2019) Nanobody-Facilitated Multiparametric PET/MRI Phenotyping of Atherosclerosis. *JACC Cardiovasc. Imaging 12* (10), 2015−2026.

(93) Ferreira, C. A., Hernandez, R., Yang, Y., Valdovinos, H. F., Engle, J. W., and Cai, W. (2018) ImmunoPET of CD146 in a Murine Hindlimb Ischemia Model. *Mol. Pharmaceutics 15* (8), 3434−3441.
(94) Xu, M., Han, Y., Liu, G., Xu, Y., Duan, D., Liu, H., Du, F., Luo, P., and Liu, Z. (2018) Preclinical Study of a Fully Human Anti-PD-L1 Antibody as a Theranostic Agent for Cancer Immunotherapy. *Mol. Pharmaceutics 15* (10), 4426−4433.
(95) Wagner, M., Wuest, M., Hamann, I., Lopez-Campistrous, A., McMullen, T. P. W., and Wuest, F. (2018) Molecular Imaging of Platelet-Derived Growth Factor Receptor-Alpha (PDGFRα) in Papillary Thyroid Cancer Using Immuno-PET. *Nucl. Med. Biol. 58*, 51−58.
(96) Li, S., England, C. G., Ehlerding, E. B., Kutyreff, C. J., Engle, J. W., Jiang, D., and Cai, W. (2019) ImmunoPET Imaging of CD38 Expression in Hepatocellular Carcinoma Using 64Cu-Labeled Daratumumab. *Am. J. Transl Res. 11* (9), 6007−6015.
(97) Butch, E. R., Mead, P. E., Amador Diaz, V., Tillman, H., Stewart, E., Mishra, J. K., Kim, J., Bahrami, A., Dearling, J. L. J., Packard, A. B., et al. (2019) Positron Emission Tomography Detects In Vivo Expression of Disialoganglioside GD2 in Mouse Models of Primary and Metastatic Osteosarcoma. *Cancer Res. 79* (12), 3112−3124.
(98) Lai, J., Lu, D., Zhang, C., Zhu, H., Gao, L., Wang, Y., Bao, R., Zhao, Y., Jia, B., Wang, F., et al. (2018) Noninvasive Small-Animal Imaging of Galectin-1 Upregulation for Predicting Tumor Resistance to Radiotherapy. *Biomaterials 158*, 1−9.
(99) Jiang, J., Zhang, M., Li, G., Liu, T., Wan, Y., Liu, Z., Zhu, H., and Yang, Z. (2020) Evaluation of 64Cu Radiolabeled Anti-HPD-L1 Nb6 for Positron Emission Tomography Imaging in Lung Cancer Tumor Mice Model. *Bioorg. Med. Chem. Lett. 30* (4), 126915.
(100) Fiedler, L., Kellner, M., Oos, R., Böning, G., Ziegler, S., Bartenstein, P., Zeidler, R., Gildehaus, F. J., and Lindner, S. (2018) Fully Automated Production and Characterization of 64Cu and Proof-of-Principle Small-Animal PET Imaging Using 64Cu-Labelled CA XII Targeting 6A10 Fab. *ChemMedChem 13* (12), 1230−1237.
(101) Morad, H. O. J., Wild, A.-M., Wiehr, S., Davies, G., Maurer, A., Pichler, B. J., and Thornton, C. R. (2018) Pre-Clinical Imaging of Invasive Candidiasis Using ImmunoPET/MR. *Front. Microbiol. 9*, 1996.
(102) Honndorf, V. S., Wiehr, S., Rolle, A.-M., Schmitt, J., Kreft, L., Quintanilla-Martinez, L., Kohlhofer, U., Reischl, G., Maurer, A., Boldt, K., et al. (2016) Preclinical Evaluation of the Anti-Tumor Effects of the Natural Isoflavone Genistein in Two Xenograft Mouse Models Monitored by [18F]FDG, [18F]FLT, and [64Cu]NODAGA-Cetuximab Small Animal PET. *Oncotarget 7* (19), 28247−28261.
(103) van Dijk, L. K., Yim, C.-B., Franssen, G. M., Kaanders, J. H. A. M., Rajander, J., Solin, O., Grönroos, T. J., Boerman, O. C., and Bussink, J. (2016) PET of EGFR with 64Cu-Cetuximab-F(Ab′) 2 in Mice with Head and Neck Squamous Cell Carcinoma Xenografts. *Contrast Media Mol. Imaging 11* (1), 65−70.
(104) Davies, G., Rolle, A. M., Maurer, A., Spycher, P. R., Schillinger, C., Solouk-Saran, D., Hasenberg, M., Weski, J., Fonslet, J., Dubois, A., et al. (2017) Towards Translational ImmunoPET/MR Imaging of Invasive Pulmonary Aspergillosis: The Humanised Monoclonal Antibody JF5 Detects Aspergillus Lung Infections in Vivo. *Theranostics 7* (14), 3398−3414.
(105) Wiehr, S., Warnke, P., Rolle, A.-M., Schütz, M., Oberhettinger, P., Kohlhofer, U., Quintanilla-Martinez, L., Maurer, A., Thornton, C., Boschetti, F., et al. (2016) New Pathogen-Specific ImmunoPET/MR Tracer for Molecular Imaging of a Systemic Bacterial Infection. *Oncotarget 7* (10), 10990−11001.
(106) Song, I. H., Lee, T. S., Park, Y. S., Lee, J. S., Lee, B. C., Moon, B. S., An, G. Il, Lee, H. W., Kim, K. Il, Lee, Y. J., et al. (2016) Immuno-PET Imaging and Radioimmunotherapy of 64Cu-/177Lu-Labeled Anti-EGFR Antibody in Esophageal Squamous Cell Carcinoma Model. *J. Nucl. Med. 57* (7), 1105−1111.
(107) Yoshii, Y., Yoshimoto, M., Matsumoto, H., Tashima, H., Iwao, Y., Takuwa, H., Yoshida, E., Wakizaka, H., Yamaya, T., Zhang, M.-R., et al. (2018) Integrated Treatment Using Intraperitoneal Radioimmunotherapy and Positron Emission Tomography-Guided Surgery with 64Cu-Labeled Cetuximab to Treat Early- and Late-Phase Peritoneal Dissemination in Human Gastrointestinal Cancer Xenografts. *Oncotarget 9* (48), 28935−28950.
(108) Yoshii, Y., Matsumoto, H., Yoshimoto, M., Oe, Y., Zhang, M.-R., Nagatsu, K., Sugyo, A., Tsuji, A. B., and Higashi, T. (2019) 64Cu-Intraperitoneal Radioimmunotherapy: A Novel Approach for Adjuvant Treatment in a Clinically Relevant Preclinical Model of Pancreatic Cancer. *J. Nucl. Med. 60* (10), 1437−1443.
(109) Tolmachev, V., Grönroos, T. J., Yim, C.-B., Garousi, J., Yue, Y., Grimm, S., Rajander, J., Perols, A., Haaparanta-Solin, M., Solin, O., et al. (2018) Molecular Design of Radiocopper-Labelled Affibody Molecules. *Sci. Rep. 8* (1), 6542.
(110) Čepa, A., Rálić, J., Král, V., Paurová, M., Kučka, J., Humajová, J., Lázníček, M., and Lebeda, O. (2018) In Vitro Evaluation of the Monoclonal Antibody 64Cu-IgG M75 against Human Carbonic Anhydrase IX and Its in Vivo Imaging. *Appl. Radiat. Isot. 133*, 9−13.
(111) Dearling, J. L. J., Paterson, B. M., Akurathi, V., Betanzos-Lara, S., Treves, S. T., Voss, S. D., White, J. M., Huston, J. S., Smith, S. V., Donnelly, P. S., et al. (2015) The Ionic Charge of Copper-64 Complexes Conjugated to an Engineered Antibody Affects Biodistribution. *Bioconjugate Chem. 26* (4), 707−717.
(112) Kramer-Marek, G., Shenoy, N., Seidel, J., Griffiths, G. L., Choyke, P., and Capala, J. (2011) 68Ga-DOTA-Affibody Molecule for in Vivo Assessment of HER2/Neu Expression with PET. *Eur. J. Nucl. Med. Mol. Imaging 38* (11), 1967−1976.
(113) Eichendorff, S., Svendsen, P., Bender, D., Keiding, S., Christensen, E. I., Deleuran, B., and Moestrup, S. K. (2015) Biodistribution and PET Imaging of a Novel [68Ga]-Anti-CD163-Antibody Conjugate in Rats with Collagen-Induced Arthritis and in Controls. *Mol. Imaging Biol. 17* (1), 87−93.
(114) Xavier, C., Vaneycken, I., D'huyvetter, M., Heemskerk, J., Keyaerts, M., Vincke, C., Devoogdt, N., Muyldermans, S., Lahoutte, T., and Caveliers, V. (2013) Synthesis, Preclinical Validation, Dosimetry, and Toxicity of 68Ga-NOTA-Anti-HER2 Nanobodies for IPET Imaging of HER2 Receptor Expression in Cancer. *J. Nucl. Med. 54* (5), 776−784.
(115) Demine, S., Garcia Ribeiro, R., Thevenet, J., Marselli, L., Marchetti, P., Pattou, F., Kerr-Conte, J., Devoogdt, N., and Eizirik, D. L. (2020) A Nanobody-Based Nuclear Imaging Tracer Targeting Dipeptidyl Peptidase 6 to Determine the Mass of Human Beta Cell Grafts in Mice. *Diabetologia 63* (4), 825−836.
(116) Bala, G., Crauwels, M., Blykers, A., Remory, I., Marschall, A. L. J., Dübel, S., Dumas, L., Broisat, A., Martin, C., Ballet, S., et al. (2019) Radiometal-Labeled Anti-VCAM-1 Nanobodies as Molecular Tracers for Atherosclerosis - Impact of Radiochemistry on Pharmacokinetics. *Biol. Chem. 400* (3), 323−332.
(117) Ma, T., Sun, X., Cui, L., Gao, L., Wu, Y., Liu, H., Zhu, Z., Wang, F., and Liu, Z. (2014) Molecular Imaging Reveals Trastuzumab-Induced Epidermal Growth Factor Receptor Down-regulation in Vivo. *J. Nucl. Med. 55* (6), 1002−1007.
(118) Suman, S. K., Kameswaran, M., Pandey, U., Sarma, H. D., and Dash, A. (2019) Preparation and Preliminary Bioevaluation Studies of 68Ga-NOTA-Rituximab Fragments as Radioimmunoscintigraphic Agents for Non-Hodgkin Lymphoma. *J. Labelled Compd. Radiopharm. 62* (12), 850−859.
(119) Lv, G., Sun, X., Qiu, L., Sun, Y., Li, K., Liu, Q., Zhao, Q., Qin, S., and Lin, J. (2020) PET Imaging of Tumor PD-L1 Expression with a Highly Specific Nonblocking Single-Domain Antibody. *J. Nucl. Med. 61* (1), 117−122.
(120) Krasniqi, A., D'Huyvetter, M., Xavier, C., Van der Jeught, K., Muyldermans, S., Van Der Heyden, J., Lahoutte, T., Tavernier, J., and Devoogdt, N. (2017) Theranostic Radiolabeled Anti-CD20 SdAb for Targeted Radionuclide Therapy of Non-Hodgkin Lymphoma. *Mol. Cancer Ther. 16* (12), 2828−2839.
(121) Xavier, C., Blykers, A., Laoui, D., Bolli, E., Vaneyken, I., Bridoux, J., Baudhuin, H., Raes, G., Everaert, H., Movahedi, K., et al. (2019) Clinical Translation of [68Ga]Ga-NOTA-Anti-MMR-SdAb

https://doi.org/10.1021/acs.bioconjchem.1c00136
Bioconjugate Chem. 2021, 32, 1315−1330

for PET/CT Imaging of Protumorigenic Macrophages. *Mol. Imaging Biol. 21* (5), 898−906.
(122) Xu, B., Li, X., Yin, J., Liang, C., Liu, L., Qiu, Z., Yao, L., Nie, Y., Wang, J., and Wu, K. (2015) Evaluation of 68Ga-Labeled MG7 Antibody: A Targeted Probe for PET/CT Imaging of Gastric Cancer. *Sci. Rep. 5* (1), 8626.
(123) Zhang, X., Liu, C., Hu, F., Zhang, Y., Wang, J., Gao, Y., Jiang, Y., Zhang, Y., and Lan, X. (2018) PET Imaging of VCAM-1 Expression and Monitoring Therapy Response in Tumor with a 68Ga-Labeled Single Chain Variable Fragment. *Mol. Pharmaceutics 15* (2), 609−618.
(124) Fay, R., Gut, M., and Holland, J. P. (2019) Photoradiosynthesis of 68Ga-Labeled HBED-CC-Azepin-MetMAb for Immuno-PET of c-MET Receptors. *Bioconjugate Chem. 30* (6), 1814−1820.
(125) Ueda, M., Hisada, H., Temma, T., Shimizu, Y., Kimura, H., Ono, M., Nakamoto, Y., Togashi, K., and Saji, H. (2015) Gallium-68-Labeled Anti-HER2 Single-Chain Fv Fragment: Development and In Vivo Monitoring of HER2 Expression. *Mol. Imaging Biol. 17* (1), 102−110.
(126) Su, X., Cheng, K., Jeon, J., Shen, B., Venturin, G. T., Hu, X., Rao, J., Chin, F. T., Wu, H., and Cheng, Z. (2014) Comparison of Two Site-Specifically 18F-Labeled Affibodies for PET Imaging of EGFR Positive Tumors. *Mol. Pharmaceutics 11* (11), 3947−3956.
(127) Burley, T. A., Da Pieve, C., Martins, C. D., Ciobota, D. M., Allott, L., Oyen, W. J., Harrington, K. J., Smith, G., and Kramer-Marek, G. (2019) Affibody-Based PET Imaging to Guide EGFR-Targeted Cancer Therapy in Head and Neck Squamous Cell Cancer Models. *J. Nucl. Med. 60* (3), 353−361.
(128) Da Pieve, C., Makarem, A., Turnock, S., Maczynska, J., Smith, G., and Kramer-Marek, G. (2020) Thiol-Reactive PODS-Bearing Bifunctional Chelators for the Development of EGFR-Targeting [18F]AlF-Affibody Conjugates. *Molecules 25* (7), 1562.
(129) Cleeren, F., Lecina, J., Ahamed, M., Raes, G., Devoogdt, N., Caveliers, V., McQuade, P., Rubins, D. J., Li, W., Verbruggen, A., et al. (2017) Al18 F-Labeling Of Heat-Sensitive Biomolecules for Positron Emission Tomography Imaging. *Theranostics 7* (11), 2924−2939.
(130) Gutfilen, B., Souza, S., and Valentini, G. (2018) Copper-64: A Real Theranostic Agent. *Drug Des., Dev. Ther. 12*, 3235−3245.
(131) Bolzati, C., and Duatti, A. (2020) The Emerging Value of 64Cu for Molecular Imaging and Therapy. *Q. J. Nucl. Med. Mol. Imaging 64* (4), 329−337.
(132) Jalilian, A. R., Osso, J. A., Jr, Vera-Araujo, J., Kumar, V., Harris, M. J., Gutfilen, B., Guérin, B., Li, H., Zhuravlev, F., Chakravarty, R., et al. (2020) IAEA Contribution to the Development of 64Cu Radiopharmaceuticals for Theranostic Applications. *Q. J. Nucl. Med. Mol. Imaging 64* (4), 338−345.
(133) Boschi, A., Martini, P., Janevik-Ivanovska, E., and Duatti, A. (2018) The Emerging Role of Copper-64 Radiopharmaceuticals as Cancer Theranostics. *Drug Discovery Today 23* (8), 1489−1501.
(134) Natarajan, A. (2020) Copper-64-ImmunoPET Imaging: Bench to Bedside. *Q. J. Nucl. Med. Mol. Imaging 64* (4), 356−363.
(135) Coenen, H. H., and Ermert, J. (2021) Expanding PET-Applications in Life Sciences with Positron-Emitters beyond Fluorine-18. *Nucl. Med. Biol. 92*, 241−269.
(136) Capriotti, G., and Duatti, A. (2020) Adding 64Cu Radiopharmaceuticals to the Toolkit of Molecular Imaging. *Q. J. Nucl. Med. Mol. Imaging 64* (4), 327−328.
(137) Pasquali, M., Martini, P., Shahi, A., Jalilian, A. R., Osso, J. A., and Boschi, A. (2020) Copper-64 Based Radiopharmaceuticals for Brain Tumors and Hypoxia Imaging. *Quarterly Journal of Nuclear Medicine and Molecular Imaging 64*, 371−381.
(138) Zhou, Y., Baidoo, K. E., and Brechbiel, M. W. (2013) Mapping Biological Behaviors by Application of Longer-Lived Positron Emitting Radionuclides. *Adv. Drug Delivery Rev. 65* (8), 1098−1111.
(139) Price, E. W., and Orvig, C. (2014) Matching Chelators to Radiometals for Radiopharmaceuticals. *Chem. Soc. Rev. 43* (1), 260−290.
(140) Mortimer, J. E., Bading, J. R., Park, J. M., Frankel, P. H., Carroll, M. I., Tran, T. T., Poku, E. K., Rockne, R. C., Raubitschek, A. A., Shively, J. E., et al. (2018) Tumor Uptake of 64Cu-DOTA-Trastuzumab in Patients with Metastatic Breast Cancer. *J. Nucl. Med. 59* (1), 38−43.
(141) Lockhart, A. C., Liu, Y., Dehdashti, F., Laforest, R., Picus, J., Frye, J., Trull, L., Belanger, S., Desai, M., Mahmood, S., et al. (2016) Phase 1 Evaluation of [64Cu]DOTA-Patritumab to Assess Dosimetry, Apparent Receptor Occupancy, and Safety in Subjects with Advanced Solid Tumors. *Mol. Imaging Biol. 18* (3), 446−453.
(142) Guo, X., Zhu, H., Zhou, N., Chen, Z., Liu, T., Liu, F., Xu, X., Jin, H., Shen, L., Gao, J., et al. (2018) Noninvasive Detection of HER2 Expression in Gastric Cancer by 64Cu-NOTA-Trastuzumab in PDX Mouse Model and in Patients. *Mol. Pharmaceutics 15* (11), 5174−5182.
(143) Bailly, C., Gouard, S., Guérard, F., Chalopin, B., Carlier, T., Faivre-Chauvet, A., Remaud-Le Saëc, P., Bourgeois, M., Chouin, N., Rbah-Vidal, L., et al. (2019) What Is the Best Radionuclide for Immuno-PET of Multiple Myeloma? A Comparison Study Between 89Zr- and 64Cu-Labeled Anti-CD138 in a Preclinical Syngeneic Model. *Int. J. Mol. Sci. 20* (10), 2564.
(144) Halime, Z., Frindel, M., Camus, N., Orain, P.-Y., Lacombe, M., Chérel, M., Gestin, J.-F., Faivre-Chauvet, A., and Tripier, R. (2015) New Synthesis of Phenyl-Isothiocyanate C-Functionalised Cyclams. Bioconjugation and 64Cu Phenotypic PET Imaging Studies of Multiple Myeloma with the Te2a Derivative. *Org. Biomol. Chem. 13* (46), 11302−11314.
(145) Cooper, M. S., Ma, M. T., Sunassee, K., Shaw, K. P., Williams, J. D., Paul, R. L., Donnelly, P. S., and Blower, P. J. (2012) Comparison of 64Cu-Complexing Bifunctional Chelators for Radioimmunoconjugation: Labeling Efficiency, Specific Activity, and in Vitro/in Vivo Stability. *Bioconjugate Chem. 23* (5), 1029−1039.
(146) Farleigh, M., Pham, T. T., Yu, Z., Kim, J., Sunassee, K., Firth, G., Forte, N., Chudasama, V., Baker, J. R., and Long, N. J. (2021) New Bifunctional Chelators Incorporating Dibromomaleimide Groups for Radiolabeling of Antibodies with Positron Emission Tomography Imaging Radioisotopes. *Bioconjugate Chem.*, 1 DOI: 10.1021/acs.bioconjchem.0c00710.
(147) Diebolder, P., Mpoy, C., Scott, J., Huynh, T. T., Fields, R., Spitzer, D., Bandara, N., and Rogers, B. E. (2021) Preclinical Evaluation of an Engineered Single-Chain Fragment Variable-Fragment Crystallizable Targeting Human CD44. *J. Nucl. Med. 62* (1), 137−143.
(148) Zhao, J., Wen, X., Li, T., Shi, S., Xiong, C., Wang, Y. A., and Li, C. (2020) Concurrent Injection of Unlabeled Antibodies Allows Positron Emission Tomography Imaging of Programmed Cell Death Ligand 1 Expression in an Orthotopic Pancreatic Tumor Model. *ACS Omega 5* (15), 8474−8482.
(149) Case, B. A., Kruziki, M. A., Stern, L. A., and Hackel, B. J. (2018) Evaluation of Affibody Charge Modification Identified by Synthetic Consensus Design in Molecular PET Imaging of Epidermal Growth Factor Receptor. *Mol. Syst. Des. Eng. 3* (1), 171−182.
(150) Tolmachev, V., Yim, C.-B., Rajander, J., Perols, A., Karlström, A. E., Haaparanta-Solin, M., Grönroos, T. J., Solin, O., and Orlova, A. (2017) Comparative Evaluation of Anti-HER2 Affibody Molecules Labeled with 64 Cu Using NOTA and NODAGA. *Contrast Media Mol. Imaging 2017*, 1−12.
(151) Schjoeth-Eskesen, C., Nielsen, C. H., Heissel, S., Højrup, P., Hansen, P. R., Gillings, N., and Kjaer, A. (2015) [64Cu]-Labelled Trastuzumab: Optimisation of Labelling by DOTA and NODAGA Conjugation and Initial Evaluation in Mice. *J. Labelled Compd. Radiopharm. 58* (6), 227−233.
(152) Ghosh, S. C., Pinkston, K. L., Robinson, H., Harvey, B. R., Wilganowski, N., Gore, K., Sevick-Muraca, E. M., and Azhdarinia, A. (2015) Comparison of DOTA and NODAGA as Chelators for 64Cu-Labeled Immunoconjugates. *Nucl. Med. Biol. 42* (2), 177−183.
(153) Le Bihan, T., Navarro, A.-S., Le Bris, N., Le Saëc, P., Gouard, S., Haddad, F., Gestin, J.-F., Chérel, M., Faivre-Chauvet, A., and Tripier, R. (2018) Synthesis of C -Functionalized TE1PA and

Comparison with Its Analogues. An Example of Bioconjugation on 9E7.4 MAb for Multiple Myeloma 64Cu-PET Imaging. *Org. Biomol. Chem. 16* (23), 4261−4271.
(154) Navarro, A.-S., Le Bihan, T., Le Saëc, P., Bris, N., Le Bailly, C., Saï-Maurel, C., Bourgeois, M., Chérel, M., Tripier, R., and Faivre-Chauvet, A. (2019) TE1PA as Innovating Chelator for 64Cu Immuno-TEP Imaging: A Comparative in Vivo Study with DOTA/NOTA by Conjugation on 9E7.4 MAb in a Syngeneic Multiple Myeloma Model. *Bioconjugate Chem. 30* (9), 2393−2403.
(155) David, T., Hlinová, V., Kubíček, V., Bergmann, R., Striese, F., Berndt, N., Szöllosi, D., Kovács, T., Máthé, D., Bachmann, M., et al. (2018) Improved Conjugation, 64-Cu Radiolabeling, in Vivo Stability, and Imaging Using Nonprotected Bifunctional Macrocyclic Ligands: Bis(Phosphinate) Cyclam (BPC) Chelators. *J. Med. Chem. 61* (19), 8774−8796.
(156) Tsionou, M. I., Knapp, C. E., Foley, C. A., Munteanu, C. R., Cakebread, A., Imberti, C., Eykyn, T. R., Young, J. D., Paterson, B. M., Blower, P. J., et al. (2017) Comparison of Macrocyclic and Acyclic Chelators for Gallium-68 Radiolabelling. *RSC Adv. 7* (78), 49586−49599.
(157) Smith, D. L., Breeman, W. A. P., and Sims-Mourtada, J. (2013) The Untapped Potential of Gallium 68-PET: The next Wave of 68Ga-Agents. *Appl. Radiat. Isot. 76*, 14−23.
(158) Sörensen, J., Velikyan, I., Sandberg, D., Wennborg, A., Feldwisch, J., Tolmachev, V., Orlova, A., Sandström, M., Lubberink, M., Olofsson, H., et al. (2016) Measuring HER2-Receptor Expression In Metastatic Breast Cancer Using [68Ga]ABY-025 Affibody PET/CT. *Theranostics 6* (2), 262−271.
(159) Sandberg, D., Tolmachev, V., Velikyan, I., Olofsson, H., Wennborg, A., Feldwisch, J., Carlsson, J., Lindman, H., and Sörensen, J. (2017) Intra-Image Referencing for Simplified Assessment of HER2-Expression in Breast Cancer Metastases Using the Affibody Molecule ABY-025 with PET and SPECT. *Eur. J. Nucl. Med. Mol. Imaging 44* (8), 1337−1346.
(160) Velikyan, I., Schweighöfer, P., Feldwisch, J., Seemann, J., Frejd, F. Y., Lindman, H., and Sörensen, J. (2019) Diagnostic HER2-Binding Radiopharmaceutical, [68Ga]Ga-ABY-025, for Routine Clinical Use in Breast Cancer Patients. *Am. J. Nucl. Med. Mol. Imaging 9* (1), 12−23.
(161) Keyaerts, M., Xavier, C., Heemskerk, J., Devoogdt, N., Everaert, H., Ackaert, C., Vanhoeij, M., Duhoux, F. P., Gevaert, T., Simon, P., et al. (2016) Phase I Study of 68Ga-HER2-Nanobody for PET/CT Assessment of HER2 Expression in Breast Carcinoma. *J. Nucl. Med. 57* (1), 27−33.
(162) Nawaz, S., Mullen, G. E. D., Sunassee, K., Bordoloi, J., Blower, P. J., and Ballinger, J. R. (2017) Simple, Mild, One-Step Labelling of Proteins with Gallium-68 Using a Tris(Hydroxypyridinone) Bifunctional Chelator: A 68Ga-THP-ScFv Targeting the Prostate-Specific Membrane Antigen. *EJNMMI Res. 7* (1), 86.
(163) Brunnquell, C. L., Hernandez, R., Graves, S. A., Smit-Oistad, I., Nickles, R. J., Cai, W., Meyerand, E., Suzuki, M., and Meyerand, M. E. (2016) Uptake and Retention of Manganese Contrast Agents for PET and MRI in the Rodent Brain. *Contrast Media Mol. Imaging 11* (5), 371−380.
(164) Wooten, A. L., Aweda, T. A., Lewis, B. C., Gross, R. B., and Lapi, S. E. (2017) Biodistribution and PET Imaging of Pharmacokinetics of Manganese in Mice Using Manganese-52. *PLoS One 12* (3), No. e0174351.
(165) Saar, G., Millo, C. M., Szajek, L. P., Bacon, J., Herscovitch, P., and Koretsky, A. P. (2018) Anatomy, Functionality, and Neuronal Connectivity with Manganese Radiotracers for Positron Emission Tomography HHS Public Access. *Mol. Imaging Biol. 20* (4), 562−574.
(166) De Nardo, L., Ferro-Flores, G., Bolzati, C., Esposito, J., and Meléndez-Alafort, L. (2019) Radiation Effective Dose Assessment of [51Mn]- and [52Mn]-Chloride. *Appl. Radiat. Isot. 153* (04), 108805.
(167) Graves, S. A., Hernandez, R., Fonslet, J., England, C. G., Valdovinos, H. F., Ellison, P. A., Barnhart, T. E., Elema, D. R., Theuer, C. P., Cai, W., et al. (2015) Novel Preparation Methods of 52Mn for ImmunoPET Imaging. *Bioconjugate Chem. 26* (10), 2118−2124.
(168) Rösch, F., Herzog, H., and Qaim, S. (2017) The Beginning and Development of the Theranostic Approach in Nuclear Medicine, as Exemplified by the Radionuclide Pair 86Y and 90Y. *Pharmaceuticals 10* (4), 56.
(169) Nayak, T. K., and Brechbiel, M. W. (2011) 86Y Based PET Radiopharmaceuticals: Radiochemistry and Biological Applications. *Med. Chem. (Sharjah, United Arab Emirates) 7* (5), 380−388.
(170) Ehlerding, E. B., Ferreira, C. A., Aluicio-Sarduy, E., Jiang, D., Lee, H. J., Theuer, C. P., Engle, J. W., and Cai, W. (2018) 86/90Y-Based Theranostics Targeting Angiogenesis in a Murine Breast Cancer Model. *Mol. Pharmaceutics 15* (7), 2606−2613.
(171) Ferreira, C. A., Ehlerding, E. B., Rosenkrans, Z. T., Jiang, D., Sun, T., Aluicio-Sarduy, E., Engle, J. W., Ni, D., and Cai, W. (2020) 86/90Y-Labeled Monoclonal Antibody Targeting Tissue Factor for Pancreatic Cancer Theranostics. *Mol. Pharmaceutics 17* (5), 1697−1705.
(172) Amor-Coarasa, A., Kelly, J., Ponnala, S., Nikolopoulou, A., Williams, C., and Babich, J. (2018) 66Ga: A Novelty or a Valuable Preclinical Screening Tool for the Design of Targeted Radiopharmaceuticals? *Molecules 23* (10), 2575.
(173) Oroujeni, M., Xu, T., Gagnon, K., Rinne, S. S., Weis, J., Garousi, J., Andersson, K. G., Löfblom, J., Orlova, A., and Tolmachev, V. (2021) The Use of a Non-Conventional Long-Lived Gallium Radioisotope 66Ga Improves Imaging Contrast of EGFR Expression in Malignant Tumours Using DFO-ZEGFR:2377 Affibody Molecule. *Pharmaceutics 13* (2), 292.
(174) Rodríguez-Villafuerte, M., Hernández, E. M., Alva-Sánchez, H., Martínez-Dávalos, A., and Ávila-Rodríguez, M. A. (2019) Positron Range Effects of 66Ga in Small-Animal PET Imaging. *Phys. Medica 67*, 50−57.
(175) Radchenko, V., Meyer, C. A. L., Engle, J. W., Naranjo, C. M., Unc, G. A., Mastren, T., Brugh, M., Birnbaum, E. R., John, K. D., Nortier, F. M., et al. (2016) Separation of 44Ti from Proton Irradiated Scandium by Using Solid-Phase Extraction Chromatography and Design of 44Ti/44Sc Generator System. *J. Chromatogr. A 1477*, 39−46.
(176) Carzaniga, T. S., Auger, M., Braccini, S., Bunka, M., Ereditato, A., Nesteruk, K. P., Scampoli, P., Türler, A., and van der Meulen, N. (2017) Measurement of 43Sc and 44Sc Production Cross-Section with an 18 MeV Medical PET Cyclotron. *Appl. Radiat. Isot. 129*, 96−102.
(177) Radchenko, V., Engle, J. W., Medvedev, D. G., Maassen, J. M., Naranjo, C. M., Unc, G. A., Meyer, C. A. L., Mastren, T., Brugh, M., Mausner, L., et al. (2017) Proton-Induced Production and Radiochemical Isolation of 44Ti from Scandium Metal Targets for 44Ti/44Sc Generator Development. *Nucl. Med. Biol. 50*, 25−32.
(178) Chaple, I. F., and Lapi, S. E. (2018) Production and Use of the First-Row Transition Metal PET Radionuclides 43,44Sc, 52Mn, and 45Ti. *J. Nucl. Med. 59* (11), 1655−1659.
(179) Müller, C., Domnanich, K. A., Umbricht, C. A., and Van Der Meulen, N. P. (2018) Scandium and Terbium Radionuclides for Radiotheranostics: Current State of Development towards Clinical Application. *Br. J. Radiol. 91* (1091), 20180074.
(180) Huclier-Markai, S., Alliot, C., Kerdjoudj, R., Mougin-Degraef, M., Chouin, N., and Haddad, F. (2018) Promising Scandium Radionuclides for Nuclear Medicine: A Review on the Production and Chemistry up to *In Vivo* Proofs of Concept. *Cancer Biother.Radiopharm. 33* (8), 316−329.
(181) Talip, Z., Favaretto, C., Geistlich, S., and Meulen, N. P. (2020) van der. A Step-by-Step Guide for the Novel Radiometal Production for Medical Applications: Case Studies with 68Ga, 44Sc, 177Lu and 161Tb. *Molecules 25* (4), 966.
(182) Price, E. W., and Orvig, C. (2014) Matching Chelators to Radiometals for Radiopharmaceuticals. *Chem. Soc. Rev. 43* (1), 260−290.
(183) Majkowska-Pilip, A., and Bilewicz, A. (2011) Macrocyclic Complexes of Scandium Radionuclides as Precursors for Diagnostic and Therapeutic Radiopharmaceuticals. *J. Inorg. Biochem. 105* (2), 313−320.

https://doi.org/10.1021/acs.bioconjchem.1c00136
Bioconjugate Chem. 2021, 32, 1315−1330

(184) Honarvar, H., Müller, C., Cohrs, S., Haller, S., Westerlund, K., Karlström, A. E., van der Meulen, N. P., Schibli, R., and Tolmachev, V. (2017) Evaluation of the First 44Sc-Labeled Affibody Molecule for Imaging of HER2-Expressing Tumors. *Nucl. Med. Biol. 45*, 15−21.
(185) Chakravarty, R., Goel, S., Valdovinos, H. F., Hernandez, R., Hong, H., Nickles, R. J., and Cai, W. (2014) Matching the Decay Half-Life with the Biological Half-Life: ImmunoPET Imaging with 44Sc-Labeled Cetuximab Fab Fragment. *Bioconjugate Chem. 25* (12), 2197−2204.
(186) Vaughn, B. A., Ahn, S. H., Aluicio-Sarduy, E., Devaraj, J., Olson, A. P., Engle, J., and Boros, E. (2020) Chelation with a Twist: A Bifunctional Chelator to Enable Room Temperature Radiolabeling and Targeted PET Imaging with Scandium-44. *Chem. Sci. 11* (2), 333.
(187) Chansaenpak, K., Vabre, B., and Gabbaï, F. P. (2016) [18F]-Group 13 Fluoride Derivatives as Radiotracers for Positron Emission Tomography. *Chem. Soc. Rev. 45* (4), 954−971.
(188) Zeng, J.-L., Wang, J., and Ma, J.-A. (2015) New Strategies for Rapid 18F-Radiolabeling of Biomolecules for Radionuclide-Based In Vivo Imaging. *Bioconjugate Chem. 26* (6), 1000−1003.
(189) Bernard-Gauthier, V., Lepage, M. L., Waengler, B., Bailey, J. J., Liang, S. H., Perrin, D. M., Vasdev, N., and Schirrmacher, R. (2018) Recent Advances in 18F Radiochemistry: A Focus on B-18F, Si-18F, Al-18F, and C-18F Radiofluorination via Spirocyclic Iodonium Ylides. *J. Nucl. Med. 59* (4), 568−572.
(190) Kumar, K., and Ghosh, A. (2018) 18F-AlF Labeled Peptide and Protein Conjugates as Positron Emission Tomography Imaging Pharmaceuticals. *Bioconjugate Chem. 29*, 953−975.
(191) Fersing, C., Bouhlel, A., Cantelli, C., Garrigue, P., Lisowski, V., and Guillet, B. (2019) A Comprehensive Review of Non-Covalent Radiofluorination Approaches Using Aluminum [18F]Fluoride: Will [18F]AlF Replace 68Ga for Metal Chelate Labeling? *Molecules 24* (16), 2866.
(192) McBride, W. J., Sharkey, R. M., Karacay, H., D'Souza, C. A., Rossi, E. A., Laverman, P., Chang, C.-H., Boerman, O. C., and Goldenberg, D. M. (2009) A Novel Method of 18F Radiolabeling for PET. *J. Nucl. Med. 50* (6), 991−998.
(193) Shetty, D., Choi, S. Y., Jeong, J. M., Lee, J. Y., Hoigebazar, L., Lee, Y.-S., Lee, D. S., Chung, J.-K., Lee, M. C., and Chung, Y. K. (2011) Stable Aluminium Fluoride Chelates with Triazacyclononane Derivatives Proved by X-Ray Crystallography and 18F-Labeling Study. *Chem. Commun. 47* (34), 9732.
(194) Basuli, F., Zhang, X., Williams, M. R., Seidel, J., Green, M. V., Choyke, P. L., Swenson, R. E., and Jagoda, E. M. (2018) One-Pot Synthesis and Biodistribution of Fluorine-18 Labeled Serum Albumin for Vascular Imaging. *Nucl. Med. Biol. 62*−*63*, 63−70.
(195) McBride, W. J., Sharkey, R. M., and Goldenberg, D. M. (2013) Radiofluorination Using Aluminum-Fluoride (Al18F). *EJNMMI Res. 3* (1), 36.
(196) Tolmachev, V., and Orlova, A. (2020) Affibody Molecules as Targeting Vectors for PET Imaging. *Cancers 12* (3), 651.
(197) Cleeren, F., Lecina, J., Billaud, E. M. F., Ahamed, M., Verbruggen, A., and Bormans, G. M. (2016) New Chelators for Low Temperature Al18F-Labeling of Biomolecules. *Bioconjugate Chem. 27* (3), 790−798.
(198) Cleeren, F., Lecina, J., Bridoux, J., Devoogdt, N., Tshibangu, T., Xavier, C., and Bormans, G. (2018) Direct Fluorine-18 Labeling of Heat-Sensitive Biomolecules for Positron Emission Tomography Imaging Using the Al18F-RESCA Method. *Nat. Protoc. 13* (10), 2330−2347.
(199) Musthakahmed, A. M. S., Billaud, E., Bormans, G., Cleeren, F., Lecina, J., and Verbruggen, A. (2016) Methods for Low Temperature Fluorine-18 Radiolabeling of Biomolecules. Internation Patent WO 2016065435 a2.

https://doi.org/10.1021/acs.bioconjchem.1c00136
Bioconjugate Chem. 2021, 32, 1315−1330